UCLA
UCLA Previously Published Works

Title

Near-Surface Vortex Structure in a Tornado and in a Sub-Tornado-Strength Convective-Storm Vortex Observed by a Mobile, W-Band Radar during VORTEX2

Permalink

https://escholarship.org/uc/item/5q19p4ww

Journal

Monthly Weather Review, 141(11)

ISSN

0027-0644

Authors

Tanamachi, Robin L
Bluestein, Howard B
Xue, Ming
et al.

Publication Date

2013-11-01

DOI

10.1175/mwr-d-12-00331.1

Peer reviewed

eScholarship.org Powered by the California Digital Library
University of California

Near-Surface Vortex Structure in a Tornado and in a Sub-Tornado-Strength Convective-Storm Vortex Observed by a Mobile, W-Band Radar during VORTEX2

ROBIN L. TANAMACHI,*,+ HOWARD B. BLUESTEIN,# MING XUE,* WEN-CHAU LEE,@ KRZYSZTOF A. ORZEL,& STEPHEN J. FRASIER,& AND ROGER M. WAKIMOTO@

* *Center for Analysis and Prediction of Storms, and School of Meteorology, University of Oklahoma, Norman, Oklahoma*
# *School of Meteorology, University of Oklahoma, Norman, Oklahoma*
@ *National Center for Atmospheric Research, Boulder, Colorado*
& *Microwave Remote Sensing Laboratory, University of Massachusetts, Amherst, Amherst, Massachusetts*

(Manuscript received 14 November 2012, in final form 22 May 2013)

ABSTRACT

As part of the Second Verification of the Origins of Rotation in Tornadoes Experiment (VORTEX2) field campaign, a very high-resolution, mobile, W-band Doppler radar collected near-surface (≤200 m AGL) observations in an EF-0 tornado near Tribune, Kansas, on 25 May 2010 and in sub-tornado-strength vortices near Prospect Valley, Colorado, on 26 May 2010. In the Tribune case, the tornado's condensation funnel dissipated and then reformed after a 3-min gap. In the Prospect Valley case, no condensation funnel was observed, but evidence from the highest-resolution radars in the VORTEX2 fleet indicates multiple, sub-tornado-strength vortices near the surface, some with weak-echo holes accompanying Doppler velocity couplets. Using high-resolution Doppler radar data, the authors document the full life cycle of sub-tornado-strength vortex beneath a convective storm that previously produced tornadoes. The kinematic evolution of these vortices, from genesis to decay, is investigated via ground-based velocity track display (GBVTD) analysis of the W-band velocity data. It is found that the azimuthal velocities in the Tribune tornado fluctuated in concert with the (dis)appearance of the condensation funnel. However, the dynamic pressure drop associated with the retrieved azimuthal winds was not sufficient to account for the condensation funnel. In the Prospect Valley case, the strongest and longest-lived sub-tornado-strength vortex exhibited similar azimuthal velocity structure to the Tribune tornado, but had weaker azimuthal winds. In both cases, the radius of maximum azimuthal wind was inversely related to the wind speed, and changes in the axisymmetric azimuthal component of velocity were consistent with independent indicators of vortex intensification and decay.

1. Introduction

Tornadoes exhibit substantial variability in longevity, strength, and structure among one another and throughout their own individual life cycles. This diversity, along with increased availability of novel observations of atmospheric vortices, blurs the boundaries of any exclusive, universal definition of a tornado. Concerted efforts to collect high-resolution Doppler radar data in tornadoes have contributed to an improved understanding of vortex variability. In this study, we explore the weak end of the tornado spectrum [≤ (enhanced Fujita) EF-1] by analyzing two similar vortices that occurred one day apart and were sampled by the same instruments. One of these vortices was unequivocally a tornado, by a standard glossary definition [''A violently rotating column of air, in contact with the surface, pendant from a cumuliform cloud, and often (but not always) visible as a funnel cloud''; Glickman 2000], by the accounts of witnesses, and by a previously used, radar-based criterion (Alexander and Wurman 2008). The second vortex possessed a similar set of radar-measured characteristics, including diameter, duration, and wind speed, but did not result in any tornado reports. Therefore, while this vortex satisfied a radar-based criterion for a tornado, it failed to satisfy established human observer criteria (funnel cloud, debris cloud, or

+ Current affiliation: NOAA/National Severe Storms Laboratory, Norman, Oklahoma.

Corresponding author address: Robin L. Tanamachi, NOAA/National Severe Storms Laboratory, 120 David L. Boren Blvd., Norman, OK 73072.
E-mail: rtanamachi@ou.edu

DOI: 10.1175/MWR-D-12-00331.1

© 2013 American Meteorological Society

Downloaded from http://journals.ametsoc.org/mwr/article-pdf/4300712/mwr-d-12-00331_1.pdf by guest on 10 June 2020

surface damage) for a tornado. Rather than trying to narrowly define—or even redefine—what constitutes a tornado, we offer our findings as a testimonial to vortex diversity.

Retrieval of the near-surface (≤200 m AGL) azimuthal and radial winds in tornadoes remains a challenging problem. Although mobile Doppler radars can provide remote measurements of wind speeds, they only observe the along-beam component of the flow (i.e., the Doppler velocity, denoted V_r). A relatively small feature such as a tornado (diameter ~1000 m or less) may be poorly resolved by conventional radar systems with relatively wide beam widths (i.e., >~1°) and/or at long range, since the azimuthal width of a radar gate increases with increasing range from the radar. In those instances for which a tornado can be at least marginally resolved by a Doppler radar, low-level (≤1 km AGL) V_r observations of tornadoes generally consist of a persistent (lifetime ≥1 min), compact (misoscale), relatively intense Doppler velocity couplet called a vortex signature (VS; Browning and Donaldson 1963). The VS is often collocated with a weak-echo hole (WEH) and/or is near the convergence of a spiraling reflectivity structure (i.e., relatively high-reflectivity filaments coiling around the VS). While there is no generally accepted velocity threshold delimiting tornadic from nontornadic vortices, one suggested threshold used in a number of studies based on Doppler on Wheels (DOW; Wurman et al. 1997) mobile radar data is a 40 m s^{-1} difference between the peak winds on the outbound and inbound sides of the couplet (e.g., Alexander and Wurman 2008; Marquis et al. 2012; Kosiba et al. 2013). This value corresponds to an instantaneous, vortex-relative azimuthal velocity of 20 m s^{-1}, falling close to the estimated wind speeds at the low end of both the Fujita (Fujita 1971) and enhanced Fujita (McDonald and Mehta 2006) scales of tornado intensity (instantaneous gust of 18 m s^{-1} and 3-s gust of 29 m s^{-1}, respectively). This threshold was found to work well for automated detection of tornadic VSs in large datasets (Alexander 2010). In this study, we use this threshold for comparison purposes.

Some of the efforts to retrieve 2D (for single-elevation data) and 3D (for multiple-elevation data) wind fields in atmospheric vortices from Doppler velocity data are summarized by Tanamachi et al. (2007). Typically, vortex-centered azimuthal and radial velocity components are retrieved. In previous studies, radial and azimuthal winds were retrieved in tornadoes observed by mobile Doppler radar using the ground-based velocity track display (GBVTD; Lee et al. 1999) technique (Bluestein et al. 2003b; Lee and Wurman 2005; Bluestein et al. 2007; Tanamachi et al. 2007; Kosiba et al. 2008; Kosiba and Wurman 2010; Metzger et al. 2011; Chan et al. 2012; Wakimoto et al. 2012). In some of these studies, swirl ratio and vertical velocities were calculated from 3D retrievals of flow just outside of the vortex core. The GBVTD technique has also been applied to high-resolution radar data collected in weaker convective vortices, specifically dust devils (Snyder et al. 2006). Retrieved vortex parameters (e.g., radius of maximum wind, or RMW) in the 5 June 1999 Bassett, Nebraska, tornado (hereafter the Bassett tornado; Bluestein et al. 2003b) and 15 May 1999 Stockton, Kansas, tornado (hereafter the Stockton tornado; Tanamachi et al. 2007) led to the inference that tornadoes exhibit at least two modes of intensification (steady versus decreasing RMW) and two modes of decay (increasing versus decreasing RMW).

In this study, we apply the GBVTD technique to retrieve winds in high-resolution Doppler velocity observations of a tornado observed near Tribune, Kansas, on 25 May 2010 and a sub-tornado-strength, convective storm vortex (SCV) near Prospect Valley, Colorado, on 26 May 2010. We emphasize that we do not seek to define a new class of atmospheric vortex with the SCV terminology. The vortices described herein are not dynamically distinct from tornadoes, but they contain weaker winds. We simply require a descriptive label for a vortex that appears to exist at the fuzzy lower boundary of what constitutes a tornado. The SCVs described in this manuscript had many of the same radar data characteristics as a tornado, including a persistent (≥1 min) reflectivity spiral, WEH, and VS, and occurred in an expected location for a tornado (e.g., in or near the hook echo region of a supercell). However, they did not meet human observer criteria for a tornado at any point during their life cycles. Such a SCV would likely not be accompanied by traditional visual indicators of a tornado (such as a condensation funnel or dust/debris cloud) because its winds were weak.

There are other radar-documented instances of SCVs. Bluestein et al. (2001) documented similar weak vortices observed by the University of Massachusetts–Amherst (UMass) W-band radar in the hook echoes of two different supercells in 2000. A nontornadic VS with a WEH was also observed along a gust front connected to the Bassett tornado (Bluestein et al. 2003a, their Fig. 10). Wurman and Kosiba (2008) presented DOW data collected in multiple misovortices beneath the mesocyclones of a 2000 tornadic storm near Oklaunion, Texas, and a 2008 tornadic storm near Stratford, Texas. A separate, nontornadic VS was also observed in the interlude between two tornadoes in the 29 May 2004 Geary, Oklahoma, storm (J. Wurman 2012, personal communication). To the best of the authors' knowledge, this paper contains the first presentation of the full life

Downloaded from http://journals.ametsoc.org/mwr/article-pdf/4300712/mwr-d-12-00331_1.pdf by guest on 10 June 2020

cycle of an SCV using high-resolution Doppler radar data collected beneath a supercell that previously produced tornadoes.

As in Bluestein et al. (2003b) and Tanamachi et al. (2007), the analyzed observations were collected by researchers from the University of Oklahoma (OU) and UMass using the UMass W-band (3.2-mm wavelength), mobile Doppler radar (UMass W-band radar hereafter; Bluestein and Pazmany 2000; Tsai et al. 2008). This radar, which has an exceptionally narrow beamwidth (0.18°) and a range resolution of 30 m, collected near-surface, single-elevation scans in tornadic supercells on 25 and 26 May 2010 as part of the Second Verification of the Origins of Rotation in Tornadoes Experiment (VORTEX2; Wurman et al. 2012). In both cases, the UMass W-band data and velocity retrievals cover the geneses of the tornado and SCVs. Data collection began at least 30 s prior to the appearance of a WEH and VS.

Questions guiding this study are as follows: Are there significant differences in the near-surface structures of the vortices observed by UMass W band on 25 May and 26 May? How are the GBVTD-retrieved winds related to the visual appearance of the vortex? What do the GBVTD-retrieved winds indicate about the ''modes'' of vortex intensification and decay in these two cases? Are radar-based and human observer criteria for a tornado consistent and exclusive, or can the same vortex satisfy one but not the other?

In section 2, the VORTEX2 operations and radar data collected by the UMass W band on 25 and 26 May 2010 are described. Section 3 covers radar data quality control, objective analysis, and application of the GBVTD technique. The results of the GBVTD analyses are illustrated and discussed in section 4. In section 5, we summarize the study, compare the two cases, and offer some parting thoughts.

2. Data collection

During VORTEX2, the mission of the UMass W-band radar, which had the highest spatial resolution of all the radars in the VORTEX2 fleet, was to collect near-surface Doppler radar observations in the hook echo regions of supercells. Since W-band electromagnetic waves attenuate rapidly in precipitation, and the peak transmitted power of the UMass W-band was only 600 W (57 dBm) in 2010, the UMass W-band maximum usable range was only 12.3 km. The intrinsic unambiguous velocity of the UMass W-band radar is only $\pm 4\,\mathrm{m\,s^{-1}}$. However, the effective unambiguous velocity was expanded to $\pm 38\,\mathrm{m\,s^{-1}}$ via use of a dual pulse repetition frequency (PRF) or dual pulse repetition time (PRT) technique (Doviak et al. 1976; Sirmans et al. 1976). The update time interval (~20 s) was a function of the sector width (typically ~90°–120°) and scan speed (typically $\sim 5°–6°\,\mathrm{s^{-1}}$), both of which were manually controlled by the radar operator.

a. 25 May 2010: Tornado near Tribune, Kansas

On 25 May 2010, an isolated supercell (''the Tribune storm'')[1] produced several tornadoes as it tracked from southeast Colorado into western Kansas (Monteverdi et al. 2010), including at least four landspouts observed by one of the authors (H. Bluestein). The VORTEX2 team targeted and intercepted this storm from 2300 to 0100 UTC on 26 May, collecting data in two tornadoes that it produced near the town of Tribune, Kansas. UMass W band deployed 23 km west of Tribune at 2310 UTC, scanning the hook region of the Tribune storm (which was about 8 km north of UMass W band) at an elevation angle of 0.7°, or about 100 m AGL at the tornado. At 2314 UTC, a funnel cloud (funnel 1) extended downward to contact the ground briefly, lasting 3 minutes before dissipating (Fig. 1a). It was followed by another, wider, cloud-to-ground condensation funnel (funnel 2) at 2320 UTC that also lasted 3 minutes (Fig. 1b). A reflectivity spiral, WEH likely generated by centrifuging (Dowell et al. 2005) (Fig. 2), and VS (Fig. 3) are all present in the UMass W-band data continuously from 2314 to 2324 UTC. We therefore consider the two condensation funnels to be separate visual incarnations of the same tornado. Maximum inbound and outbound velocities measured by UMass W band in the first funnel were -22 and $+18\,\mathrm{m\,s^{-1}}$ ($\pm 3\,\mathrm{m\,s^{-1}}$), respectively (Fig. 3b); in the second funnel, they were -24 and $+28\,\mathrm{m\,s^{-1}}$ (Fig. 3d). Therefore, both funnels met the Alexander and Wurman (2008) tornado criterion. Winds closer to the ground may have been stronger (Burgess et al. 2002; Lee and Wurman 2005; Wurman and Alexander 2005; Kosiba and Wurman 2010; Wurman et al. 2013).

A VORTEX2 photogrammetry team (Wakimoto et al. 2011; Atkins et al. 2012; Wakimoto et al. 2012), collocated with a mobile X-band phased array radar (MWR-05XP; Bluestein et al. 2010) 3 km south of UMass W band, took high-quality digital photographs of the entire life cycle of the Tribune tornado (e.g., Fig. 4a), while MWR-05XP collected volume scans of its parent mesocyclone (e.g., Fig. 5a). Photogrammetric analyses generated from these images permit direct comparison between the visual appearance of the storm and data collected by other instruments (in this case, mobile

[1] This storm is also informally called the Towner, Colorado, storm, in reference to a ghost town a few miles west of Tribune that is closer to the locations of the earliest tornadoes.

Downloaded from http://journals.ametsoc.org/mwr/article-pdf/4300712/mwr-d-12-00331_1.pdf by guest on 10 June 2020

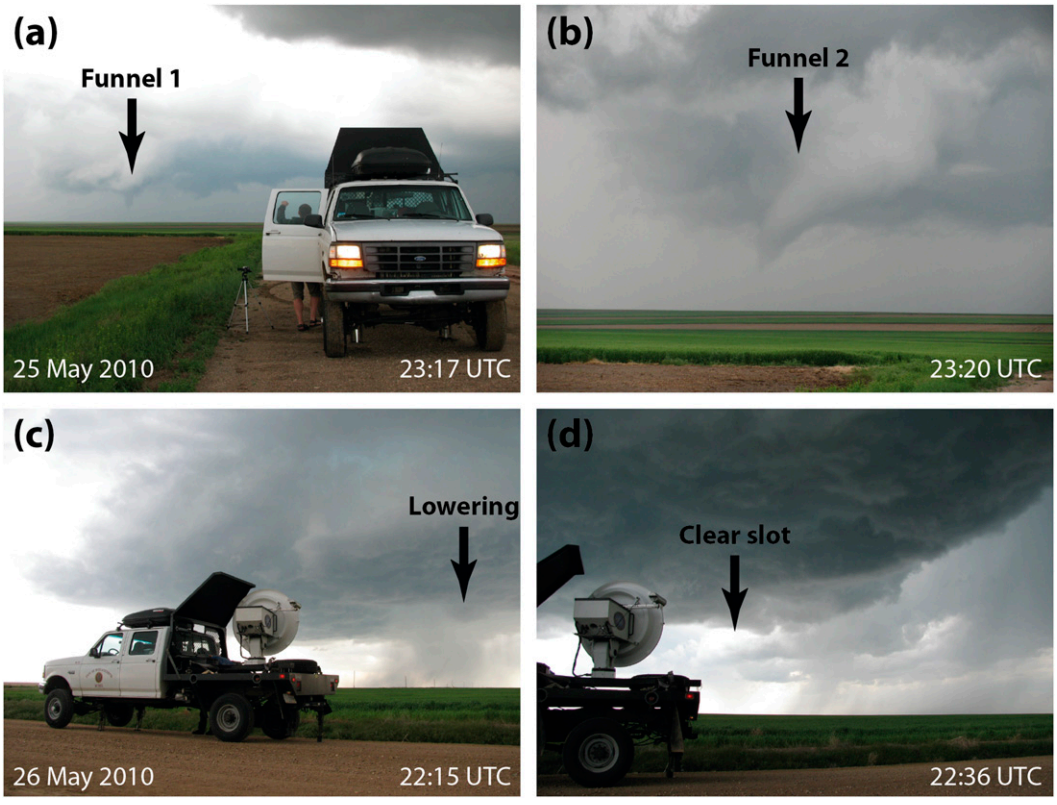

FIG. 1. The UMass W-band radar collects data in (a),(b) an EF-0 tornado in the Tribune, KS, supercell on 25 May 2010 (view toward the north) and (c),(d) the hook echo region of the Prospect Valley, CO, supercell on 26 May 2010 (view is toward the west). Photographs © R. Tanamachi.

radars; e.g., Fig. 4b). The reader is referred to Wakimoto et al. (2011) for a description of the photogrammetry methods used during VORTEX2.

b. *26 May 2010: SCV 5 near Prospect Valley, Colorado*

The Prospect Valley storm, which formed east of Denver, Colorado, tracked slowly (at 5–6 m s^{-1}) toward the northeast and remained fairly isolated for most of its life span. Between 1930 and 2110 UTC, spotters reported at least four tornadoes, prompting the National Weather Service (NWS) to issue a series of tornado warnings.

The VORTEX2 teams initially targeted this storm north of Denver International Airport, near Prospect Valley, Colorado. The slow storm motion and relatively flat terrain east of Prospect Valley made the storm an easy target for most VORTEX2 platforms. Teams converged on the storm in southern Weld County and began collecting coordinated data sets at 2150 UTC. Many teams, including at least 10 ground-based mobile Doppler radars, collected an hour or more of continuous data. Teams observed a shallow, bowl-shaped lowering of the cloud base that persisted for more than 30 min (Fig. 1c), but no tornado or funnel cloud was observed or reported. Operations ended at 0041 UTC on 27 May, when the Prospect Valley storm entered an area with a poor road network. The National Weather Service (NWS) recorded no tornado reports in this storm during VORTEX2 operations (National Climatic Data Center 2011).

During field operations, the UMass W-band radar was deployed 18 km south of Wiggins, Colorado, and collected data from 2210 to 2314 UTC. Nearby telephone poles necessitated elevating the radar beam to 1.9°. During the period of greatest interest (2217–2247 UTC), this elevation angle corresponded to a height of 150–250 m AGL in the Prospect Valley storm's hook echo (which was 4–8 km away). The hook echo exhibited complex reflectivity structure, including a fine line—possibly the leading edge of the rear-flank gust front—extending eastward from the tip of the hook (Fig. 6). Some of the SCVs occurred at the intersection of the fine line and the tip of the hook echo, possibly indicating that their origins lay in shear instability along the fine line [although the exact mechanism or mechanisms of vortex

Downloaded from http://journals.ametsoc.org/mwr/article-pdf/4300712/mwr-d-12-00331_1.pdf by guest on 10 June 2020

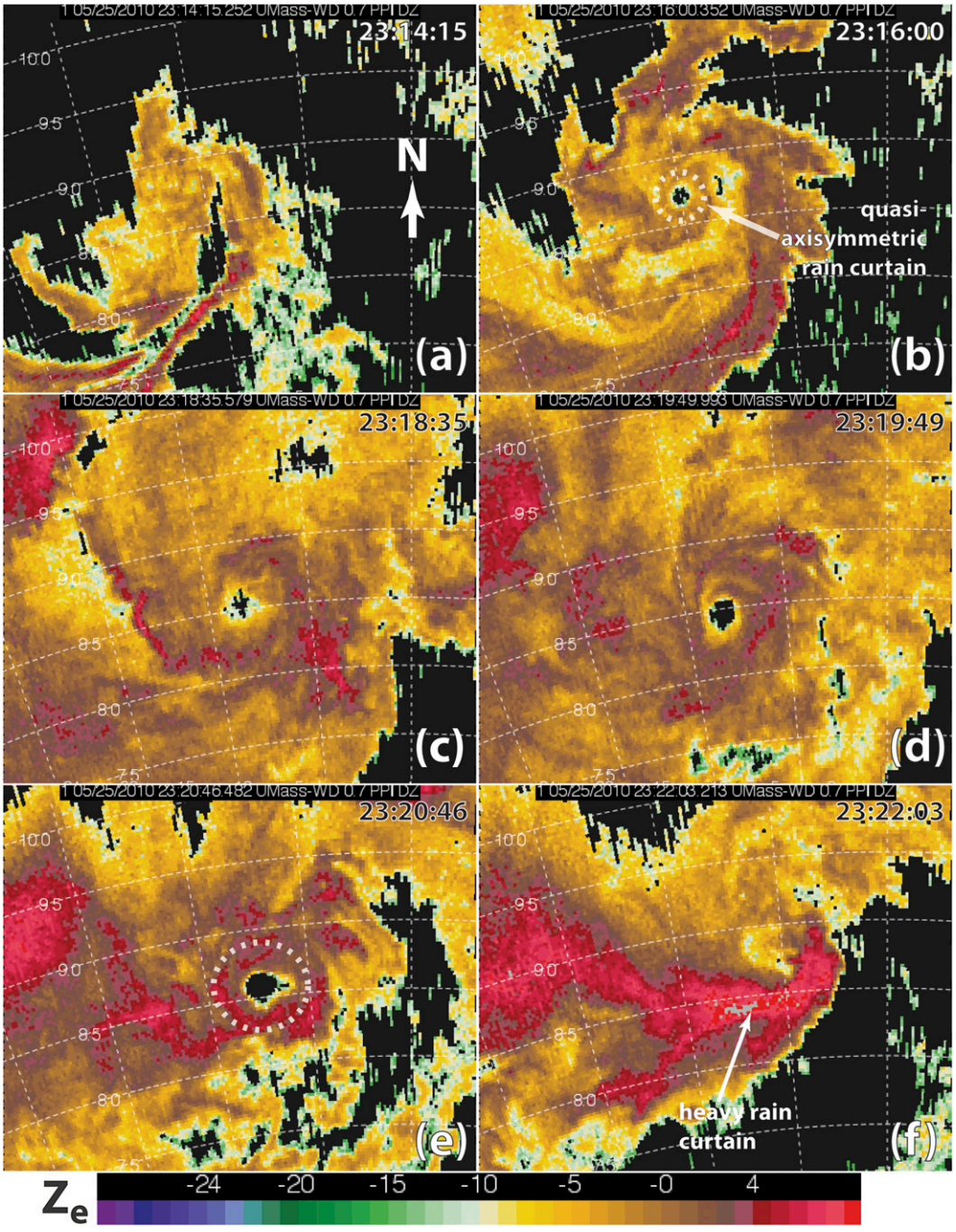

FIG. 2. Equivalent reflectivity (in dBZ_e) observed by the UMass W-band radar at an elevation angle of 0.7° in the 25 May 2010 Tribune tornado (circled) from 2314 to 2322 UTC. The images shown represent (a) tornadogenesis, (b) mature funnel 1, (c) interval between funnel 1 and funnel 2, (d) formation of funnel 2, (e) funnel 2 tilting prior to dissipation, and (f) dissipation. Quasi-axisymmetric rain curtains are indicated by dashed circles. Range rings (azimuthal spokes) are 0.5 km (10°) apart. For clarity, data associated with signal-to-noise ratio (SNR) less than −10 dB are masked.

genesis—which could also include frictional drag (Schenkman et al. 2012) or baroclinic generation and tilting of vorticity (Straka et al. 2007)—cannot be exclusively deduced from these single elevation scans]. The fine line revolved cyclonically around the tip of the hook with time, indicating the presence of larger-scale, near-surface vorticity. At least seven SCVs, all cyclonic and lasting at least 1 minute, were identified in the

Downloaded from http://journals.ametsoc.org/mwr/article-pdf/4300712/mwr-d-12-00331_1.pdf by guest on 10 June 2020

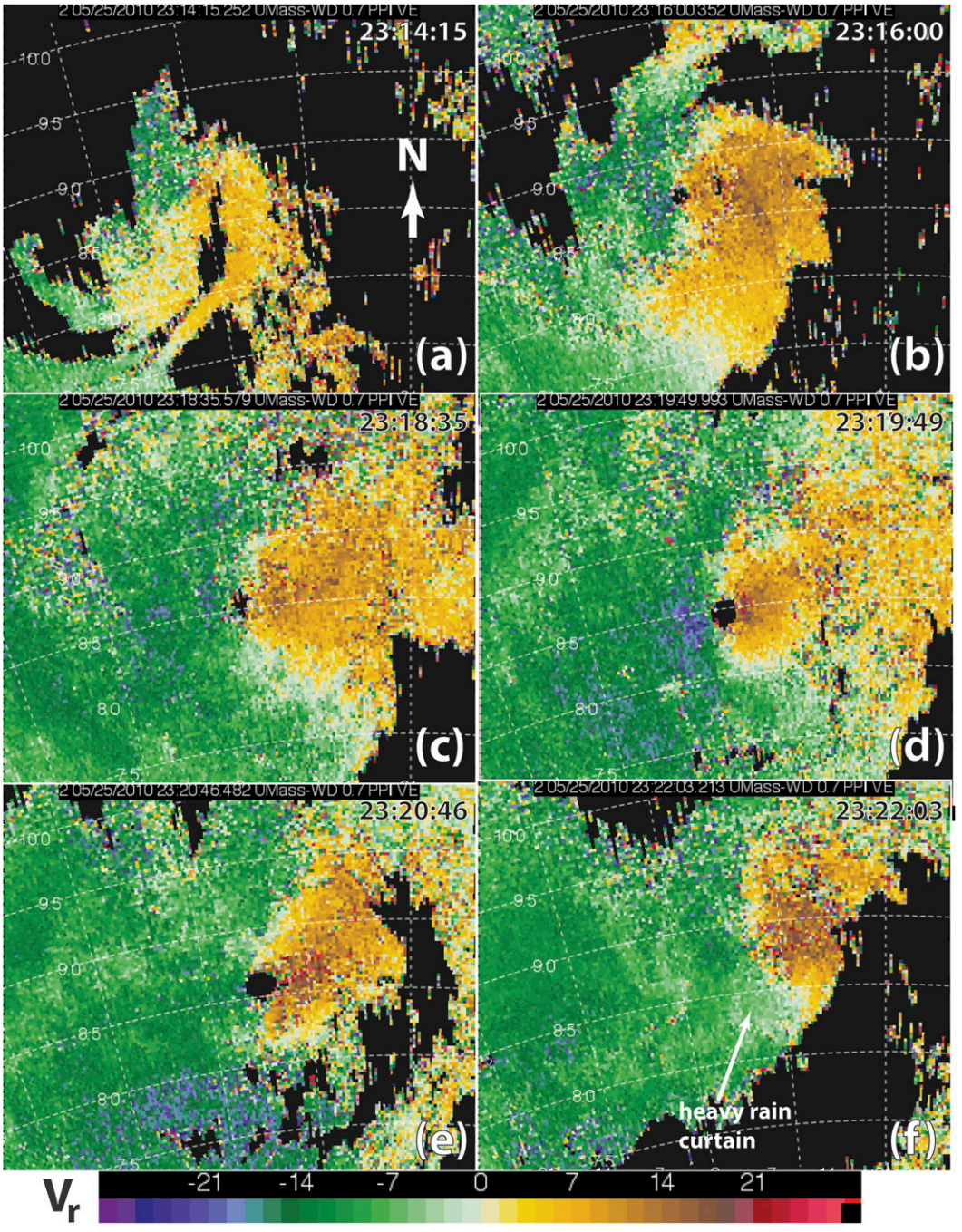

FIG. 3. As in Fig. 2, but showing Doppler velocity.

UMass W-band data (Figs. 7 and 8). The combined near-surface tracks of these SCVs (Fig. 8), as determined from UMass W-band data, resemble those of ''tornado families'' (e.g., Fujita 1960; Agee et al. 1976). The UMass W-band observations are corroborated by co-incident observations from the Texas Tech Ka-band mobile radars (not shown) (Weiss et al. 2009; Hirth et al. 2012). The SCVs consistently developed either to the southeast or south of an associated mesocyclone at 1 km AGL (LLM in Fig. 8) detected by MWR-05XP.

The strongest and longest-lived of these SCVs (5) appeared at the tip of the hook at 2234 UTC, 4.5 km from UMass W band (Fig. 9a), near the intersection with the fine line (Figs. 6c,d). In the W-band radar dataset,

Downloaded from http://journals.ametsoc.org/mwr/article-pdf/4300712/mwr-d-12-00331_1.pdf by guest on 10 June 2020

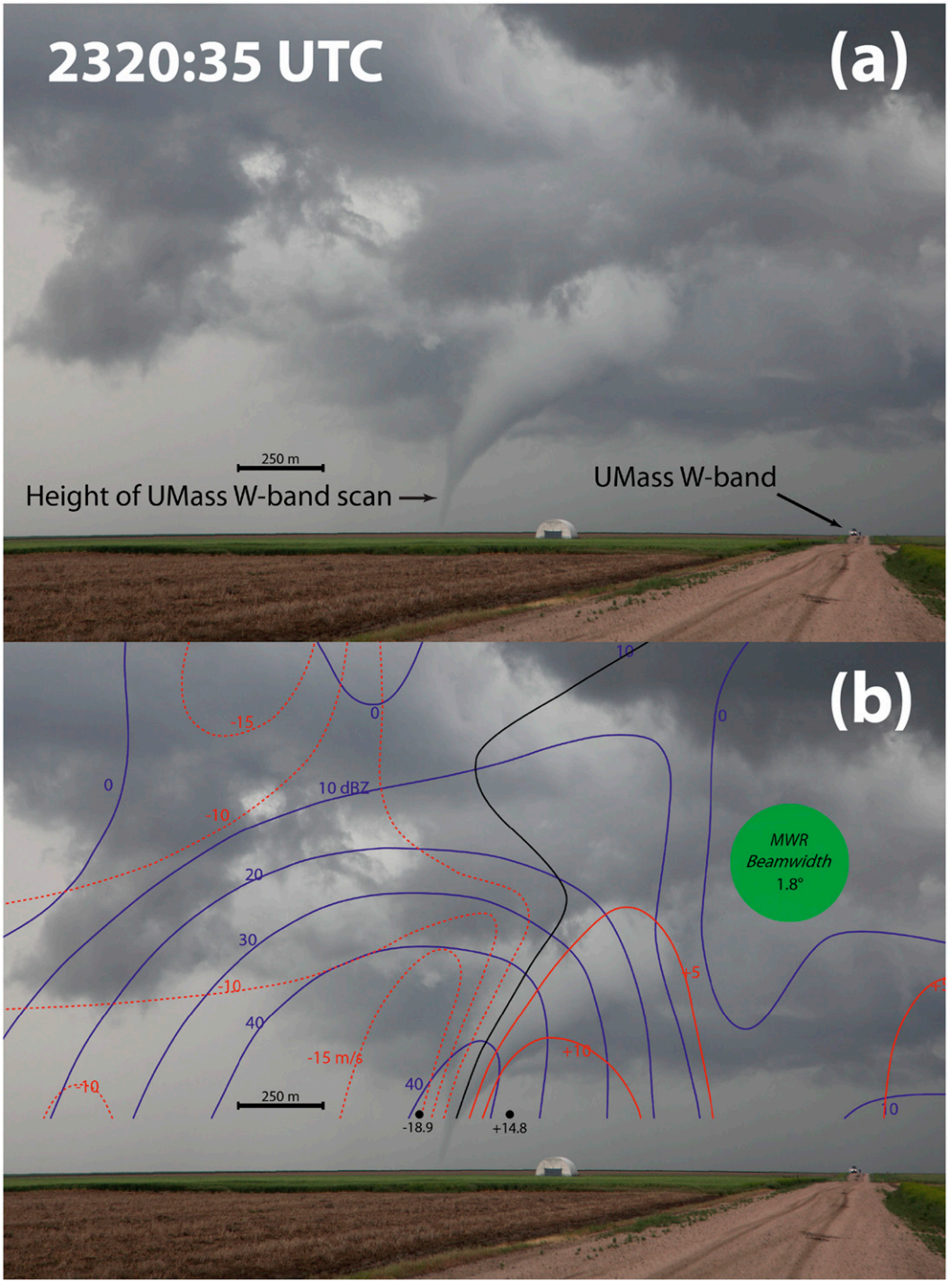

FIG. 4. (a) Photograph of funnel 2 in the Tribune tornado taken by the VORTEX2 CAMC photogrammetry team. The view is toward the north. The length scale shown is valid in the plane of the tornado. (b) As in (a), but with contours of MWR-05XP reflectivity (blue, in intervals of 10 dBZ) and Doppler velocity (red, black is the zero contour, in intervals of 5 m s^{-1}) overlaid. The two MWR-05XP velocity observations closest to the base of the tornado are plotted as black dots accompanied by velocities in m s^{-1}.

Downloaded from http://journals.ametsoc.org/mwr/article-pdf/4300712/mwr-d-12-00331_1.pdf by guest on 10 June 2020

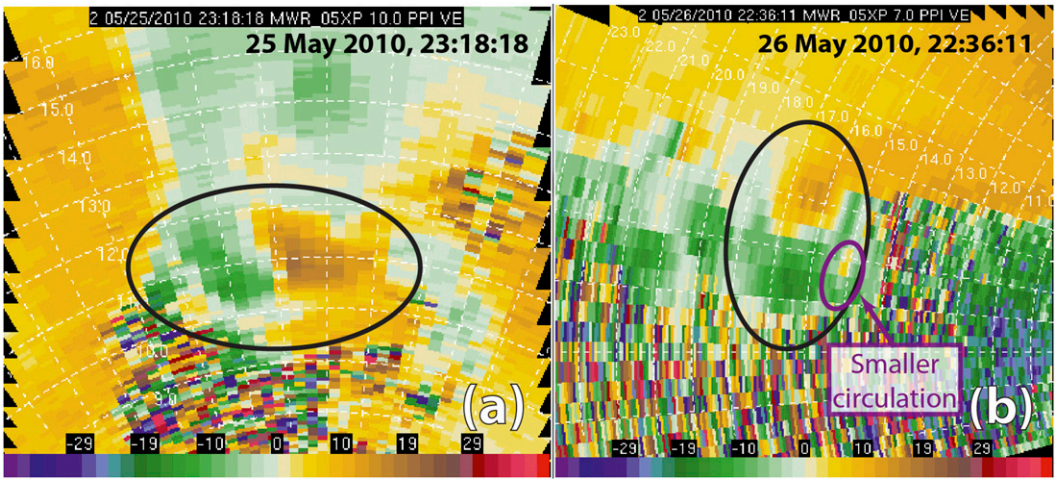

FIG. 5. MWR-05XP Doppler velocity ($m\,s^{-1}$) in mesocyclones at 2 km AGL (circled in black) in (a) the Tribune storm at 2318 UTC at an elevation angle of 10.0°, and (b) the Prospect Valley storm at 2236 UTC at an elevation angle of 7.0°. A smaller circulation believed to have controlled the motion of SCV 5 is also circled in purple. Range rings (azimuthal spokes) are 1.0 km (5°) apart.

SCV 5 bears a strong resemblance to the radar depiction of the Tribune tornado, with many similar features including a persistent WEH (Figs. 2 and 9) and VS (Figs. 3 and 10). Over the course of 8 minutes, SCV 5 revolved (Fig. 8) beneath a small circulation southeast of the low-level mesocyclone (Fig. 5b) before moving rearward (westward) and then southward with respect to the hook echo motion (Fig. 6). The maximum simultaneous inbound and outbound winds measured in SCV 5 by the UMass W-band radar were +24 and $-16\,m\,s^{-1}$ (Fig. 10d), respectively. These values are comparable with those measured in the Tribune tornado and nominally satisfy the Alexander and Wurman (2008) tornado threshold (within the estimated range of instrument error, $\pm 3\,m\,s^{-1}$). At 2242 UTC, the WEH finally filled in with precipitation and the VS weakened. We speculate that this evolution resulted from a loss of vortex stretching as SCV 5 became dislocated from its parent mesocyclone, as observations from other radars appear to indicate (e.g., Fig. 5b).

While no condensation funnel was observed in conjunction with SCV 5, this radar feature occurred in an expected location for tornadogenesis and is corroborated by other visual observations. A VORTEX2 mobile mesonet team (RN1), operating underneath the hook, reported a ''small circulation'' overhead at 2233 UTC, but their position may not have been optimal for viewing a condensation funnel. A clear slot (Lemon and Doswell 1979) is evident west-northwest of the UMass W band in a photograph taken at 2236 UTC (Fig. 1d). At 2238 UTC, another mobile mesonet (P4), just west of the hook, reported ''rising motion'' beneath the lowered cloud base as it crossed the latitude of UMass W-band. These observations coincide with SCV 5's WEH (2234–2240 UTC) in the UMass W-band data. In our GBVTD analyses, we focus principally on SCV 5 because of its similarity in size, structure, and duration (~8 min) to the Tribune tornado observed the preceding day.

3. Methodology

Because the maximum winds in the vortices did not exceed the effective maximum unambiguous velocity of UMass W band ($38\,m\,s^{-1}$), it was not necessary to manually dealias the velocity data. Clear-air reflectivity and Doppler velocity data, taken to be those associated with low signal-to-noise ratio (SNR ≤ -10 dBZ), were removed. The UMass W-band data were objectively analyzed to a Cartesian grid roughly centered on the VS using a two-pass Barnes (1964) scheme (Majcen et al. 2008). Only one vertical grid level was used because the UMass W-band data were collected at only one elevation angle. Furthermore, because of the small dimensions of the grid (2 km on a side) and shallow radar elevation angle (<2.0°), the slant of the sweep surface (<20 m) across the core diameter of the vortices (300–500 m) was ignored. During objective analysis, a time-to-space conversion, based on the subjectively estimated motion of the WEH (Fig. 8), was applied to the data in order to minimize translational distortion of the vortex (Tanamachi et al. 2007).

Koch et al. (1983) recommend objective analysis grid spacing of $\delta/2.5$, where δ is the coarsest data spacing on the analysis domain (Trapp and Doswell 2000). UMass

Downloaded from http://journals.ametsoc.org/mwr/article-pdf/4300712/mwr-d-12-00331_1.pdf by guest on 10 June 2020

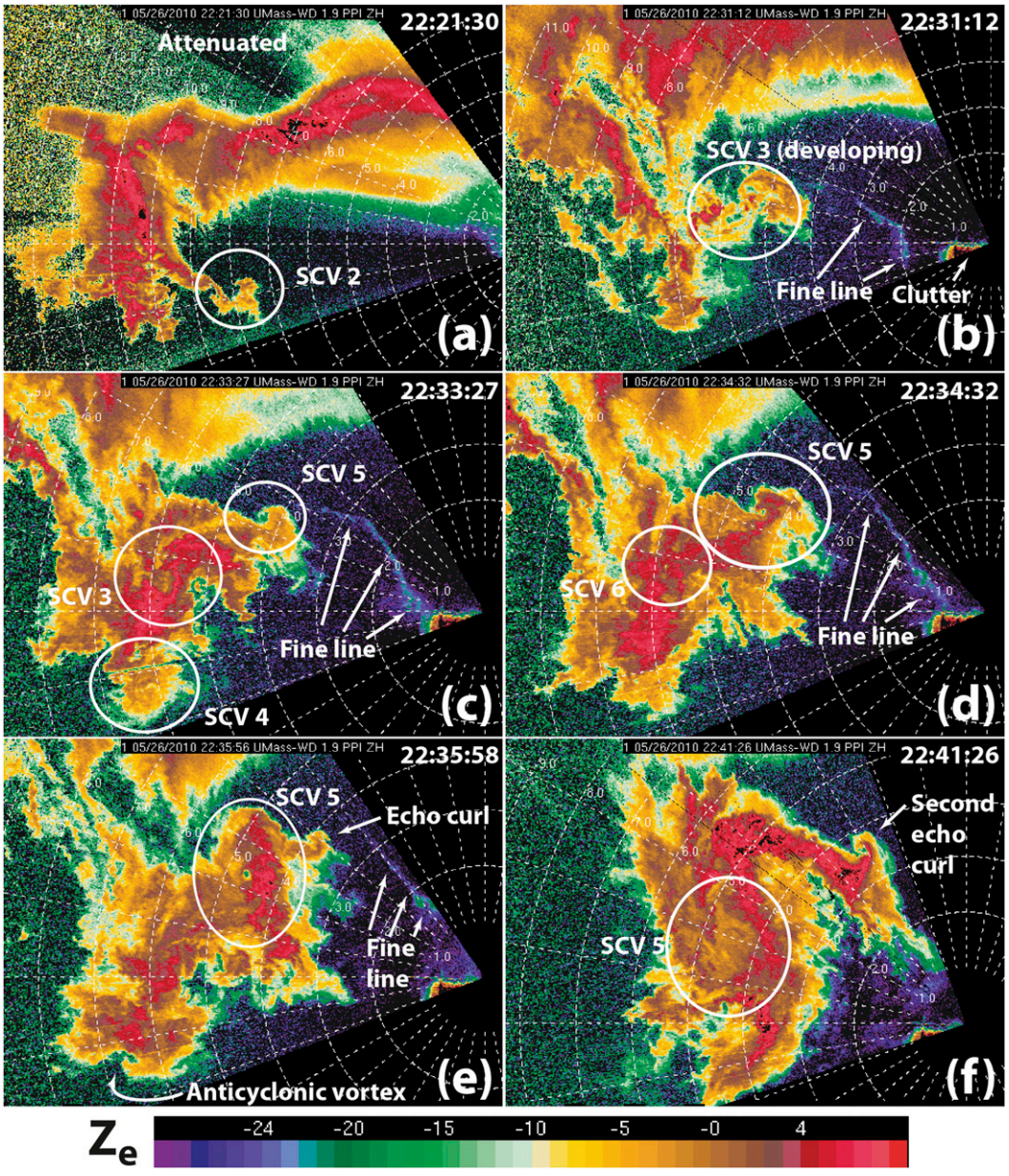

FIG. 6. Equivalent reflectivity (dBZ_e) observed by the UMass W-band radar at an elevation angle of 1.9° in the 26 May 2010 Prospect Valley storm, showing the evolution of the hook echo and gust front structures. A few echo curls not associated with significant vorticity are also annotated. Range rings (azimuthal spokes) are 1.0 km (10°) apart.

W-band range gate spacing was 24 m in both datasets. The Tribune tornado (Prospect Valley SCV 5) occurred at a range of 8.8 km (4.5 km) from UMass W band, where azimuthal resolution was 30 m (17 m). Therefore, $\delta = 30$ m (24 m) in the Tribune (Prospect Valley) case, and the corresponding horizontal grid spacing was 12 m (10 m).

For the two-pass Barnes analysis, we used a convergence parameter of $\gamma = 0.3$ (Majcen et al. 2008). Pauley and Wu (1990) recommend an optimal smoothing parameter of $\kappa_0 = (1.33\delta)^2$. For the Tribune (Prospect Valley) case, we used this formula to obtain $\kappa_0 = 1.6 \times 10^{-3}$ km^2 (1.0×10^{-3} km^2).

The Tribune data suffered from an elevated noise floor, which reduced the signal-to-noise ratio by approximately 4–6 dB relative to other UMass W-band datasets collected during VORTEX2. The radar's engineers (authors K. Orzel and S. Frasier) attribute the elevated noise floor to a temporary malfunction of the low-noise amplifier in the UMass W-band receive chain.

Downloaded from http://journals.ametsoc.org/mwr/article-pdf/4300712/mwr-d-12-00331_1.pdf by guest on 10 June 2020

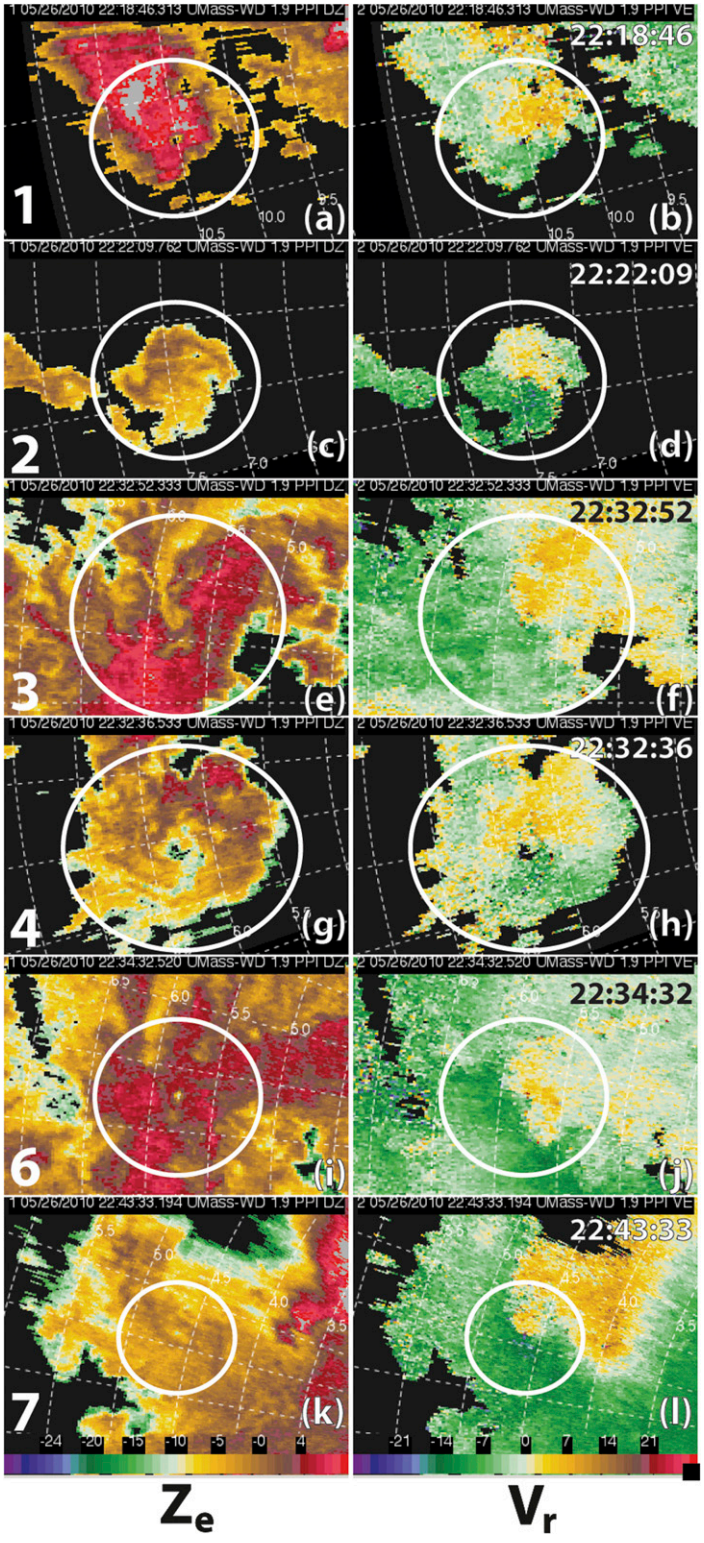

FIG. 7. (left) UMass W-band reflectivity (dBZ_e) and (right) Doppler velocity (m s^{-1}) observed in SCVs 1–4, 6, and 7 (circled) in the Prospect Valley storm's hook echo. SCV 5 (not shown) will be examined in detail later in the manuscript. For clarity, data associated with signal-to-noise ratio less than −6 dB are masked. Range rings (azimuthal spokes) are 0.5 km (5°) apart.

Downloaded from http://journals.ametsoc.org/mwr/article-pdf/4300712/mwr-d-12-00331_1.pdf by guest on 10 June 2020

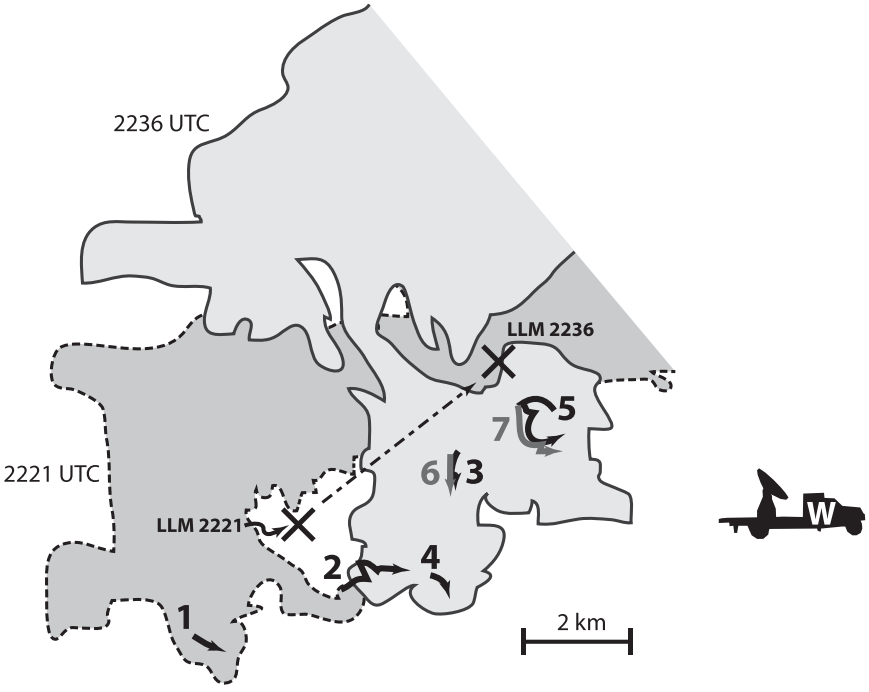

FIG. 8. Tracks of the seven SCVs detected in the Prospect Valley storm by the UMass W-band radar. For context, the tracks are overlaid on the $-10\,\mathrm{dB}Z_e$ equivalent reflectivity contour at 2221 UTC (dashed), during SCV 2, and 2236 UTC (solid), during SCV 5. Where tracks overlap, later tracks are drawn in gray. The motion of an associated low-level (1 km AGL) mesocyclone (LLM), detected by MWR-05XP, is annotated by crosses connected by a dash-dotted arrow.

This issue is unique to data collected in the Tribune deployment and did not occur in preceding or subsequent deployments of the UMass W band, including Prospect Valley. It is accepted that there will be some errors in the GBVTD analyses of the Tribune data resulting from the elevated noise floor, particularly at inner radii where SNR in the WEH is low, and the smallest number of data points are used in the Fourier analysis of the Doppler velocity data. We have excluded those analysis radii at which fewer than eight data points were available (Carbone et al. 1985). In addition, based on the results of a vortex center location sensitivity test (not shown; Bluestein et al. 2003b), we suppress analyzed velocities at radii less than 50 m. In spite of these limitations, the analyzed axisymmetric vortex structures appear similar to those of previously analyzed tornadoes. In addition, the results appear to be insensitive to grid spacing; when we repeated these analyses at coarser (30 m) grid spacing, the results (not shown) were the same. We therefore consider the analyses credible, and proceed to describe them in the next section.

The centers of the vortices were located in the objectively analyzed Doppler velocity data using the simplex center-seeking algorithm of Nelder and Mead (1965), as adapted by Lee and Marks (2000). This ''walking triangle'' algorithm maximizes vorticity in a two-dimensional wind field. The triangle (simplex) is initially centered on a first guess for the vortex center, and GBVTD-retrieved winds and vorticity are computed at each vertex. The vertices are then reflected, expanded, or contracted, and the vorticity recomputed, until the latter converges to within a specified tolerance. In some of the Tribune analyses, the center-seeking algorithm diverged significantly from the WEH, probably because of the elevated noise floor. For these analyses, a subjectively determined vortex center (usually based on the location of the VS and/or the reflectivity minimum in the WEH) was used. While both vortices moved less than 1 km in either the x or y direction (in a ground-relative sense), they both revolved counterclockwise (Fig. 11) beneath the respective parent low-level circulations (Fig. 5).

Finally, from the objectively analyzed Doppler velocity data and the vortex center at each analysis time, the GBVTD algorithm (Lee et al. 1999) calculated vortex-relative wavenumber-0 (axisymmetric), -1, -2, and -3 azimuthal velocity components (V_{T0}, V_{T1}, V_{T2}, and V_{T3}, respectively), as well as the axisymmetric radial velocity component (V_{R0}).

Downloaded from http://journals.ametsoc.org/mwr/article-pdf/4300712/mwr-d-12-00331_1.pdf by guest on 10 June 2020

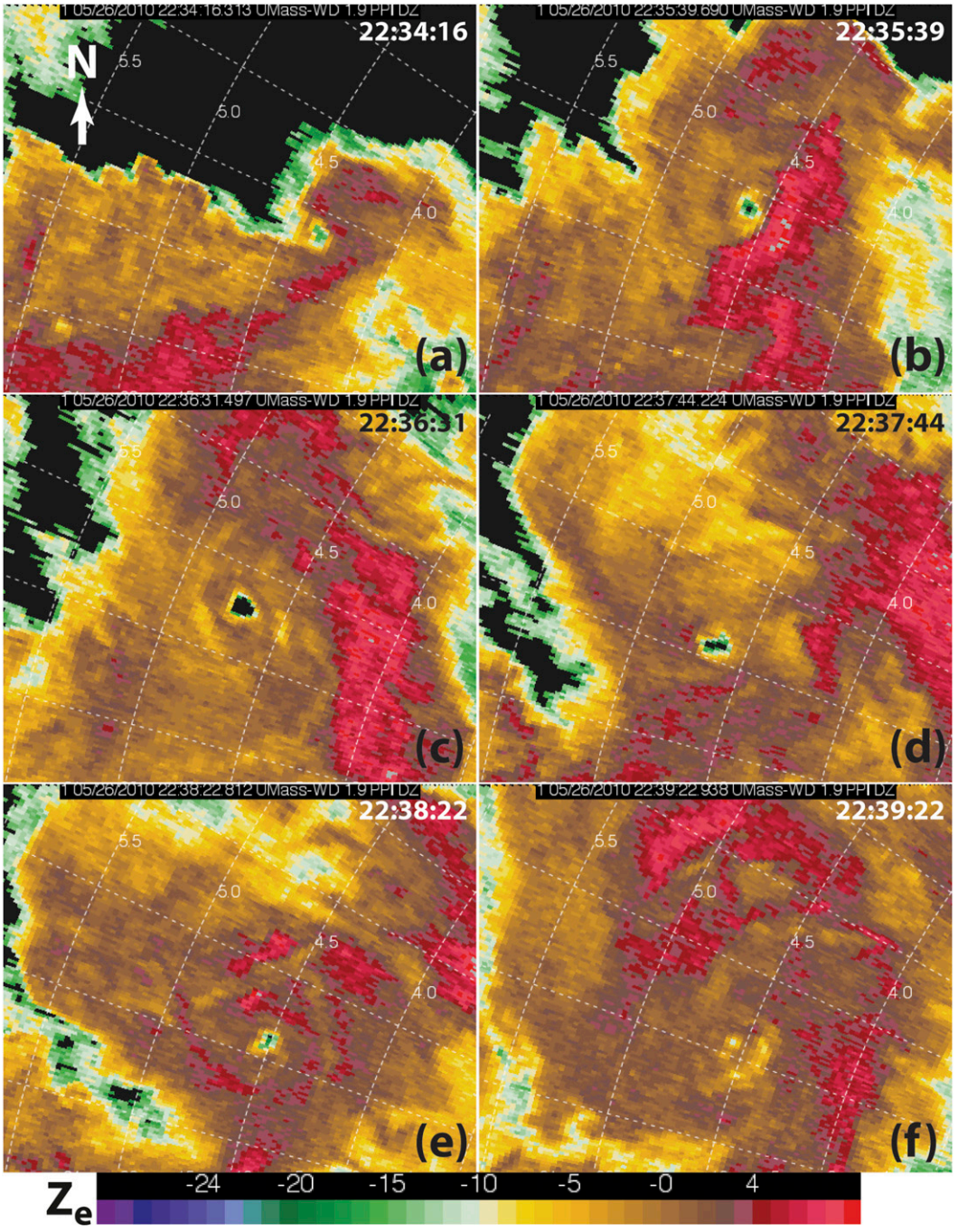

FIG. 9. As in Fig. 2, but focused on the 26 May 2010 Prospect Valley SCV 5 at an elevation angle of 1.9° from 2234 to 2239 UTC. For clarity, data associated with signal-to-noise ratio less than −6 dB are masked. These panels detail some of the data shown in Fig. 6. Range rings (azimuthal spokes) are 0.5 km (5°) apart.

4. Results

a. 25 May 2010: Tornado near Tribune, Kansas

Most of the GBVTD retrievals of azimuthal velocities in the Tribune tornado exhibited asymmetric (wavenumber 1 and 2) vortex structure (Fig. 12). [The reader is referred to Figs. 6 and 7 of Lee et al. (1999) for idealized illustrations of these features.] The V_{T1} and V_{T2} asymmetries were present at many analysis times, but were inconsistent in magnitude and orientation. Because we accounted for vortex motion in the creation of the objective analyses, translational distortion is likely

Downloaded from http://journals.ametsoc.org/mwr/article-pdf/4300712/mwr-d-12-00331_1.pdf by guest on 10 June 2020

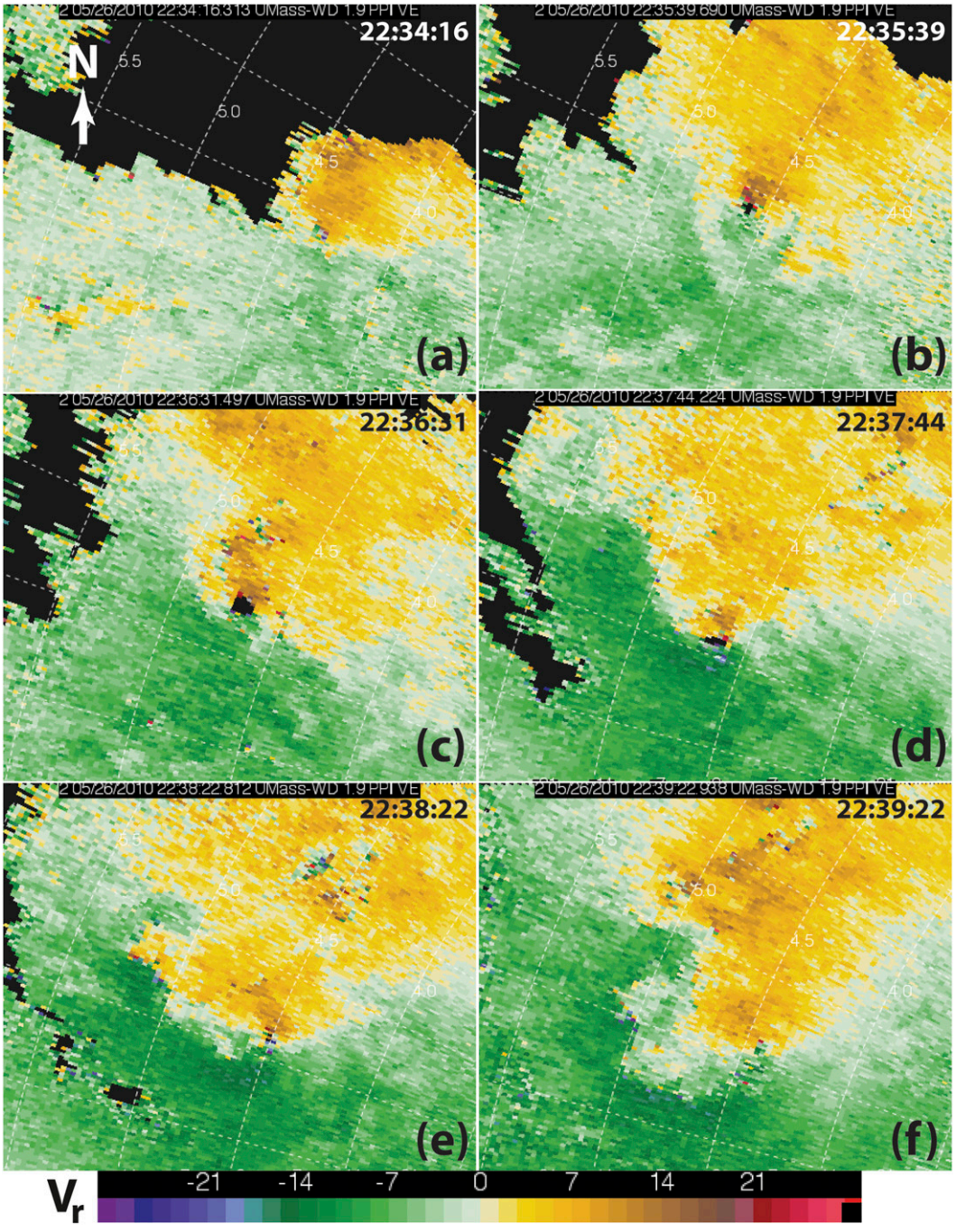

FIG. 10. As in Fig. 9, but showing Doppler velocity in m s^{-1}.

not a principal source of V_{T2} asymmetries in this case (Tanamachi et al. 2007). In addition, we did not find evidence of multiple-vortex structure in the Tribune tornado that might have resulted in V_{T1} or V_{T2} asymmetries. Finally, an otherwise identical set of GBVTD analyses generated using a slightly larger smoothing parameter ($\kappa_0 = 2.0 \times 10^{-3}$ km^2; not shown) contained smaller V_{T1} and V_{T2} asymmetries, particularly at radii less than 200 m, near the edge of the WEH. Accordingly, the authors conclude that the V_{T2} asymmetries likely resulted from remnant noise in the objective analyses.

1) AXISYMMETRIC WINDS

Hereafter, we focus on the axisymmetric component of azimuthal velocity (V_{T0}), which would have been less affected by noise and centrifuging. Peak analyzed V_{T0} in

Downloaded from http://journals.ametsoc.org/mwr/article-pdf/4300712/mwr-d-12-00331_1.pdf by guest on 10 June 2020

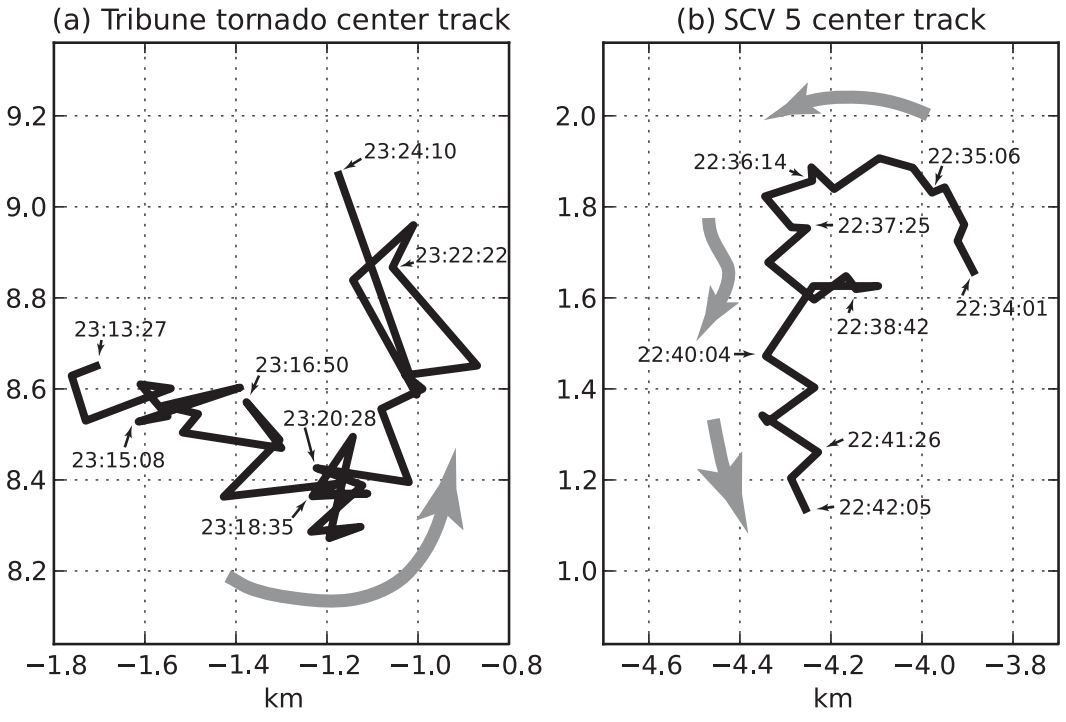

FIG. 11. Vortex center tracks for (a) the 25 May 2010 Tribune tornado (and its preceding vorticity maximum) and (b) the 26 May 2010 Prospect Valley SCV 5. Distances shown are in kilometers relative to the UMass W-band radar. Gray arrows indicate the overall direction of motion. The "wiggles" in the vortex tracks result from hysteresis of the UMass W-band antenna.

the Tribune tornado was 19 m s^{-1} at 2319:49 UTC, just as funnel 2 appeared. Higher velocities were analyzed in different parts of the tornado when higher-wavenumber components were included (Fig. 12d). The V_{T0} profiles of the Tribune tornado (Fig. 13) bore less of a resemblance to a Burgers–Rott vortex profile (Burgers 1948; Rott 1958) than those generated from previous GBVTD analyses of tornadoes (Bluestein et al. 2007; Tanamachi et al. 2007; Kosiba and Wurman 2010), except at a few specific times when the tornado was most intense (e.g., Fig. 13d). Specifically, in most of the analyses, at radii greater than 300 m, azimuthal velocities either remained constant or increased with radius rather than decaying to potential flow (e.g., Fig. 13f)—further evidence that the tornado was embedded in a larger-scale circulation at the level of the radar scan.

In general, the V_{T0} winds and associated circulation increased (decreased) at all radii in concert with the appearance (disappearance) of the tornado condensation funnel (Figs. 14 and 15). Vorticity inside a 200-m radius also exhibited this trend (Fig. 15). The WEH (taken subjectively as the area inside the −4-dBZ_e contour) was about 200 m in diameter (Fig. 16) and lasted from the first appearance of funnel 1 to the disappearance of funnel 2 (2314–2322 UTC), briefly widening to about 250 m during the time gap between the two funnels (2318 UTC).

In terms of peak V_{T0} (which occurred at 2319:49 UTC), the Tribune tornado was both wider (230-m radius) and weaker (19 m s^{-1}; F0) than either the Bassett (140 m; 30 m s^{-1}; F0) or Stockton (80 m; 45 m s^{-1}; F1) tornadoes (Bluestein et al. 2003b; Tanamachi et al. 2007). The Stockton tornado had a continuous condensation funnel throughout its life cycle, whereas the condensation funnel of the Bassett tornado was "intermittent" (Bluestein et al. 2003a), like the Tribune tornado.

We elect not to examine V_{R0} in detail at inner radii (<150 m) in this EF0 tornado because the retrievals were inconsistent in sign between analysis times and highly sensitive to vortex center location perturbations, likely a result of the elevated noise floor in this dataset and a corresponding scarcity of useable data points inside the WEH. These limitations prevent us from conclusively diagnosing the Tribune tornado as a one- or two-celled vortex (Sullivan 1959). In addition, Wakimoto et al. (2012) demonstrated that GBVTD-analyzed V_{R0} in weak tornadoes (EF2 or less) that are accompanied by weak low-level inflow is likely to be dominated by hydrometeor centrifuging at innermost (< ~200 m) radii, a conclusion supported in a subsequent modeling study (Nolan 2013).

Downloaded from http://journals.ametsoc.org/mwr/article-pdf/4300712/mwr-d-12-00331_1.pdf by guest on 10 June 2020

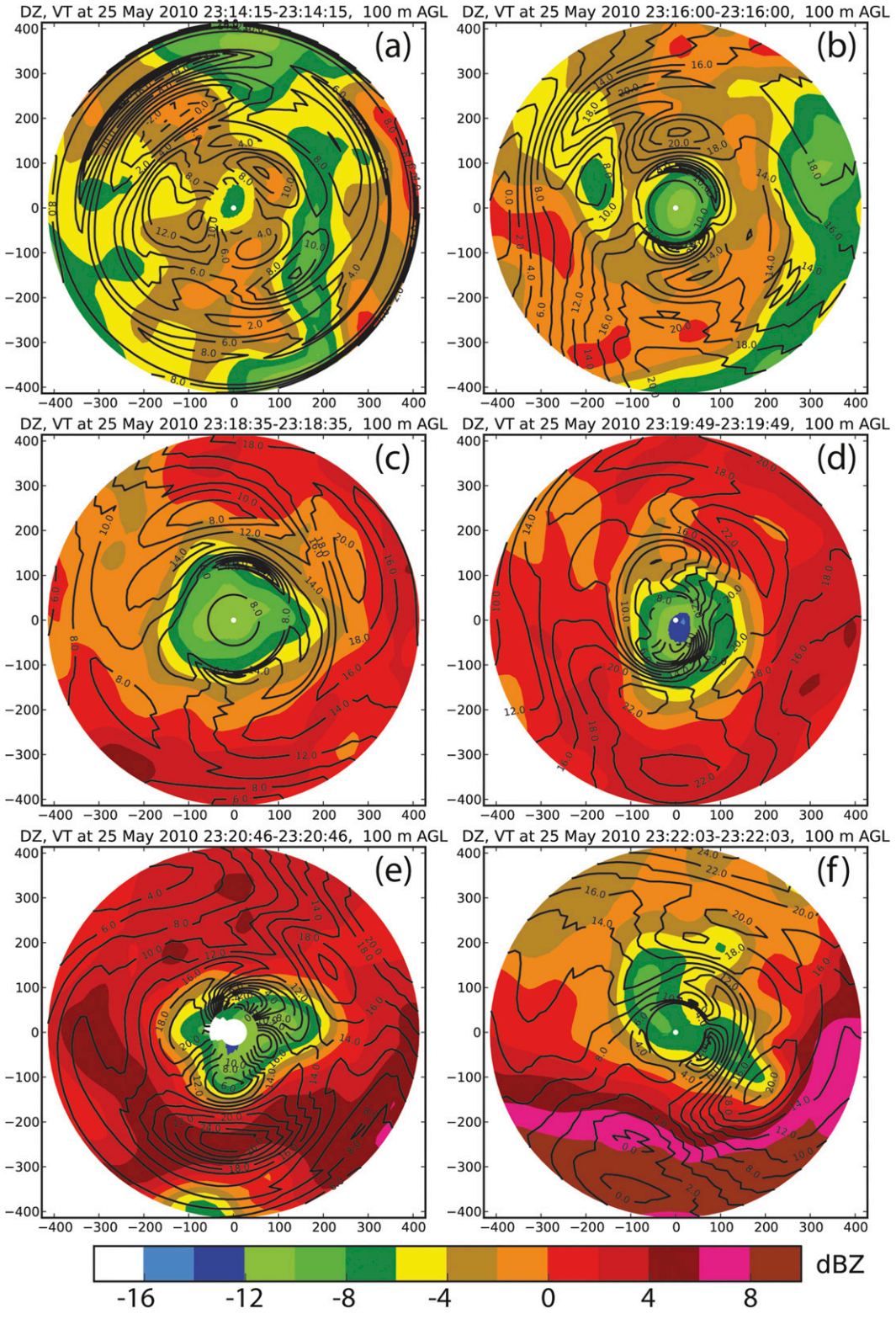

FIG. 12. UMass W-band reflectivity (filled color contours; dBZ_e) and GBVTD-analyzed azimuthal velocities (solid contours; m s^{-1}) for the 25 May 2010 Tribune tornado at (a) 2314, (b) 2316, (c) 2319, (d) 2320, (e) 2321, and (f) 2322 UTC.

Downloaded from http://journals.ametsoc.org/mwr/article-pdf/4300712/mwr-d-12-00331_1.pdf by guest on 10 June 2020

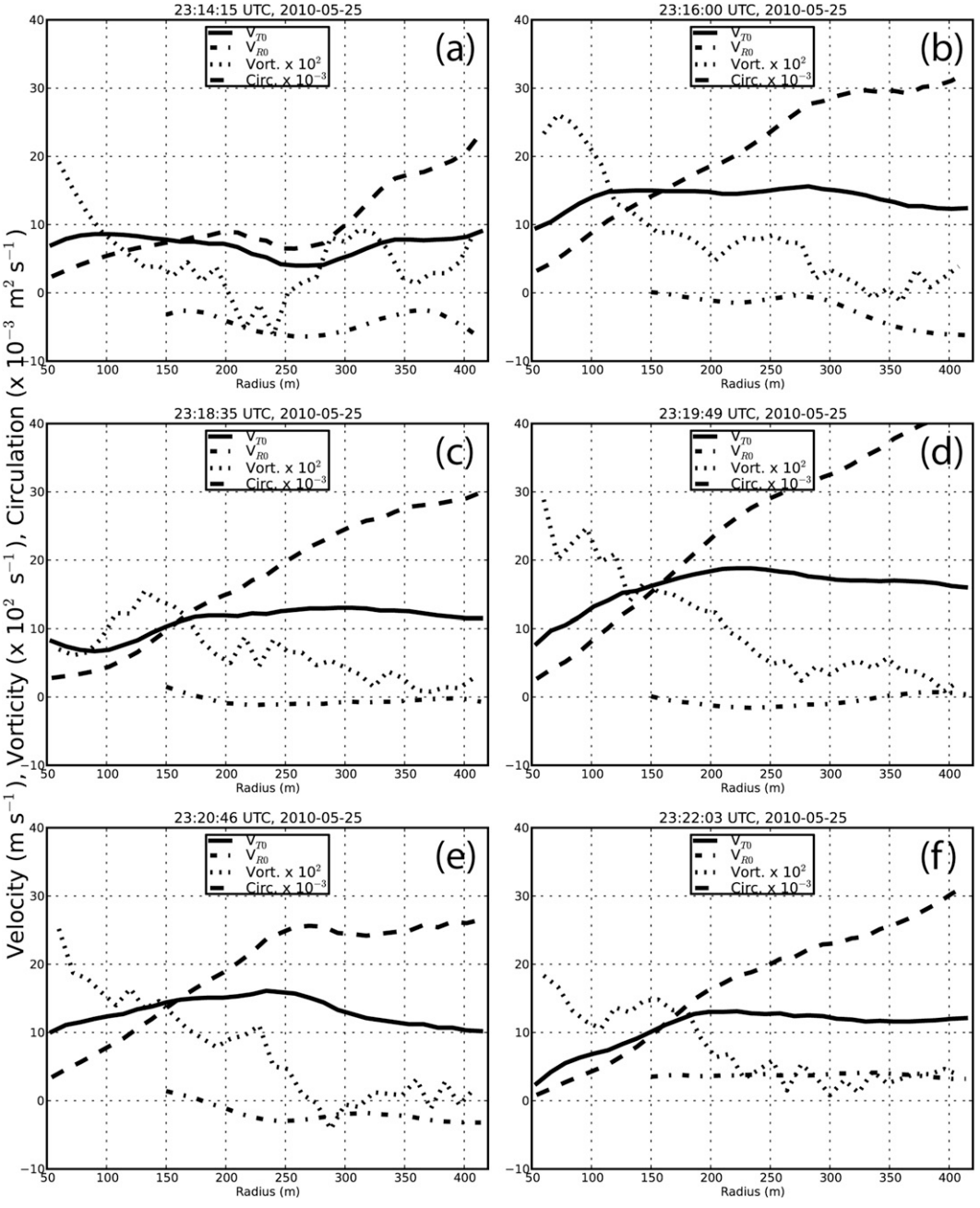

FIG. 13. GBVTD-analyzed axisymmetric components of azimuthal velocity (solid curve; m s^{-1}) and radial velocity (dash–dotted curve; m s^{-1}), vorticity (dotted curve; 10^2 s^{-1}), and circulation (dashed curve, 10^{-3} m^2 s^{-1}) as a function of radius from the analyses shown in Fig. 12. Retrieved V_{R0} inside a 150-m radius are suppressed, as they were found to be exceptionally sensitive to vortex center location error.

However, V_{R0} retrievals appear to be of adequate quality (in terms of analysis-to-analysis consistency) outside the tornado core. At radii $\geq$ 150 m, radial inflow was analyzed from 2313 to 2315 UTC as funnel 1 appeared (Fig. 13). Similarly consistent near-surface radial inflow in the intensifying tornadoes has been demonstrated by Bluestein et al. (2003b), Lee and Wurman (2005), Tanamachi et al. (2007), Kosiba and Wurman (2010), and Chan et al. (2012). Weak outflow was analyzed from the dissipation of funnel 1 (2317 UTC) to intensification of funnel 2 (2320 UTC). Weak inflow resumed as funnel 2 reached peak intensity (2320 UTC) and the dynamic pressure deficit in the vortex core increased, before again reverting to weak outflow as funnel 2 dissipated (Fig. 14). Lee and

Downloaded from http://journals.ametsoc.org/mwr/article-pdf/4300712/mwr-d-12-00331_1.pdf by guest on 10 June 2020

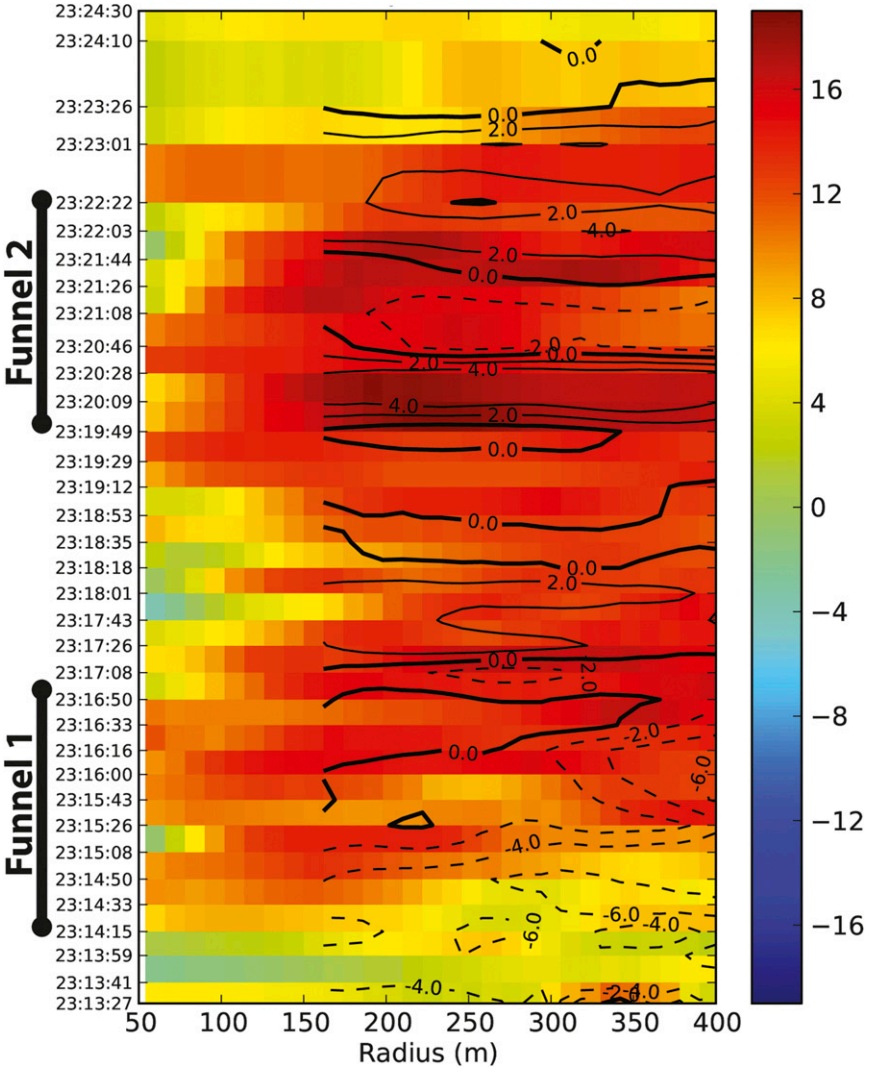

FIG. 14. Hovmöller diagram of GBVTD-analyzed V_{T0} (colored shading in m s^{-1}) and V_{R0} (black contours in intervals of 2 m s^{-1}) in the Tribune tornado as a function of radius. Visible condensation funnels are denoted on the vertical axis. Contours of V_{R0} inside 150-m radius are suppressed as in Fig. 13.

Wurman (2005), Kosiba et al. (2008), Marquis et al. (2012), Kosiba et al. (2013), and Wakimoto et al. (2012) have shown a similar reversal of near-surface radial flow outside the core of a mature or decaying tornado resulting from a secondary, "down-and-out," toroidal circulation.

2) COMPARISON WITH PHOTOGRAMMETRIC ANALYSES

MWR-05XP reflectivity and velocity data were overlaid in the plane of corresponding photographs of funnel 2 (Fig. 4b). The maximum inbound and outbound velocities measured by MWR at 150 m AGL (at its lowest elevation angle, 1.0°) were −19 and +15 m s^{-1}, respectively, in good agreement with those from UMass W band (Fig. 3e). The MWR data reflect the visible tilt toward the northeast with height of the tornado.

In the photogrammetric analyses of the Tribune tornado, condensation funnel 2 attained a maximum diameter of 30 m at the height of the UMass W-band scan (100 m AGL) at 2320:35 UTC (Fig. 4a), (approximately equal to the width of one UMass W-band range gate). Therefore, at this altitude, the condensation funnel was completely contained within the 200–300-m-wide WEH. Wakimoto et al. (2012) reached a similar conclusion after layering DOW X-band reflectivity data on photographs of the 5 June 2009 LaGrange, Wyoming, tornado. Previous observations of liquid water clouds and fog with the W-band radar yielded reflectivity values

Downloaded from http://journals.ametsoc.org/mwr/article-pdf/4300712/mwr-d-12-00331_1.pdf by guest on 10 June 2020

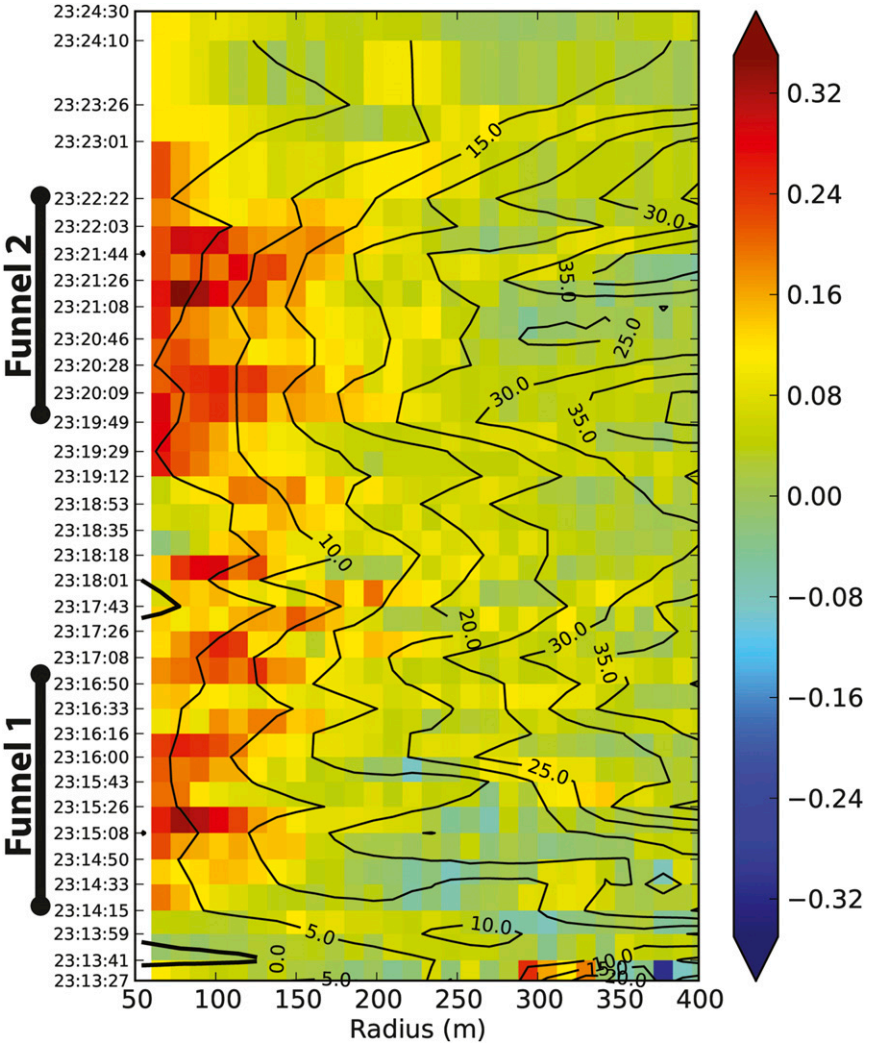

FIG. 15. As in Fig. 14, but showing vertical vorticity (colored shading in s^{-1}) and circulation (black contours at intervals of $5.0 \times 10^3 m^2 s^{-1}$).

ranging from -22 dBZ_e (the minimum detectable signal) up to 0 dBZ_e. However, funnel 2 does not appear in the W-band reflectivity field (Fig. 2e); we could not associate an individual range gate with the condensation funnel with a high degree of confidence. The lack of scatterers within the WEH would have made these inner-core winds difficult to detect. In addition, the narrowness of the condensation funnel would have made the winds in the vortex core nearly impossible to resolve with the UMass W-band radar, even with its narrow (0.18°) beamwidth. We conclude that Wakimoto et al. (2012)'s conceptual model of the WEH and condensation funnel (their Fig. 8) holds at W band as well as at X band.

3) CONDENSATION FUNNELS

We have shown that, out to a radius of at least 400 m, V_{T0} increased (decreased) when the condensation funnel appeared (disappeared). However, the condensation funnel itself cannot be explained from the GBVTD-analyzed winds alone, as will be shown below. Assuming the thermodynamic properties of ingested air remain relatively constant, a condensation funnel forms in response to increasing wind speeds and a dynamic pressure drop inside the vortex, where water vapor condenses into cloud droplets. The appearance (disappearance) of a condensation funnel, therefore, serves as a visual indicator of vortex intensification (weakening).

We obtained a crude estimate of the pressure deficit at a 50-m radius using the GBVTD-analyzed winds. We assumed the Tribune tornado was in cyclostrophic balance, that the pressure at the largest analyzed radius r_{max} (420 m in the Tribune case and 350 m in the Prospect Valley case) was representative of the near-vortex environment, and that variations in air density ρ were

Downloaded from http://journals.ametsoc.org/mwr/article-pdf/4300712/mwr-d-12-00331_1.pdf by guest on 10 June 2020

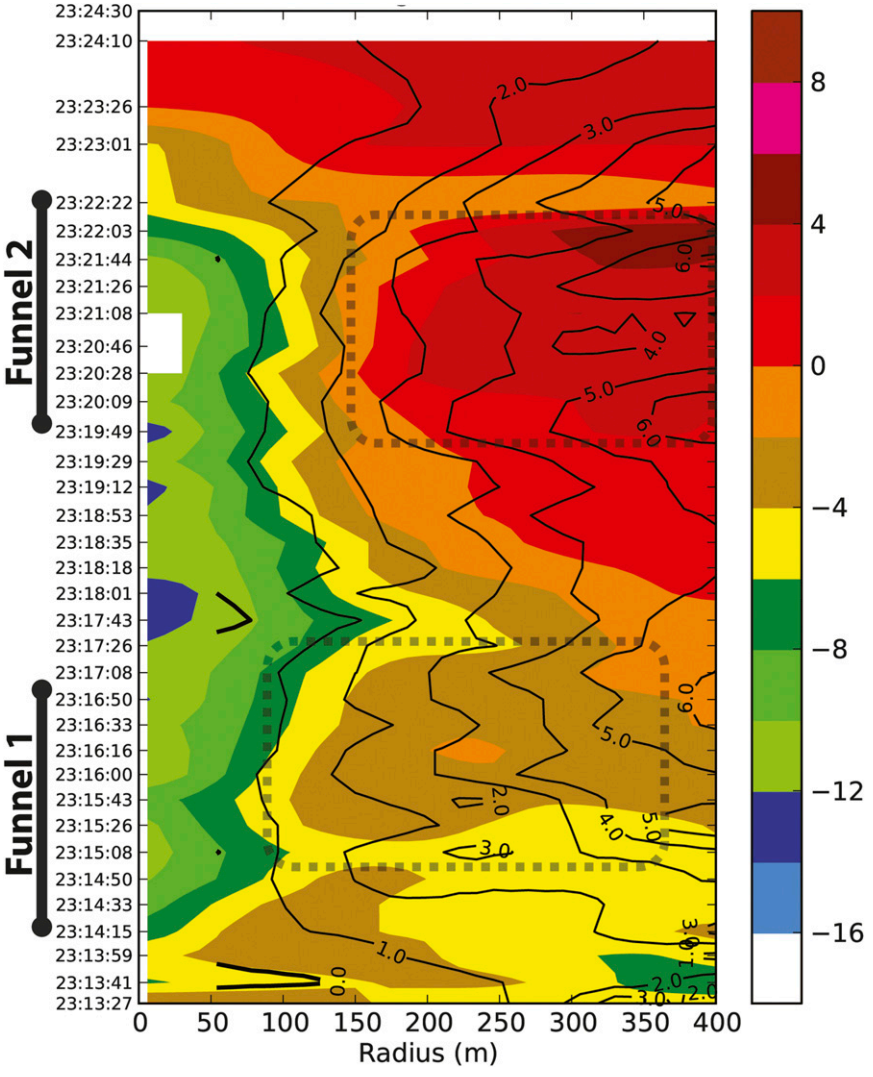

FIG. 16. As in Fig. 14, but showing azimuthally averaged equivalent reflectivity (filled color contours in dBZ_e) and angular momentum per unit mass (black contours at intervals of $1.0 \times 10^3\,\mathrm{m^2\,s^{-1}}$). Translucent dotted boxes indicate equivalent reflectivity maxima corresponding to quasi-axisymmetric rain curtains (dotted circles in Figs. 2b,e). Note that the x axis is slightly expanded relative to Fig. 14 in order to show more of the WEH.

negligible (e.g., Chan et al. 2012). Under these assumptions, the relationship between V_{T0} and pressure deficit ΔP at radius r can be expressed as

$$\Delta P(r) = \rho \int_{r_{\max}}^{r} \frac{V_{T0}^2(s)}{s}\, ds. \qquad (1)$$

Evaluating inward the integral in Eq. (1) using the trapezoidal rule and applying the ideal gas law, we find the lowest pressure and temperature deficits resulting from the $19\,\mathrm{m\,s^{-1}}$ V_{T0} winds at 2320 UTC would have been −4.8 hPa (see Fig. 18a) and −1.7°C, respectively. A sounding collected in the inflow sector of the Tribune storm (Fig. 17a) showed a well-mixed layer extending from the surface (890 hPa) to about 850 m AGL (805 hPa), with dewpoint depressions decreasing from 7.6° to 1.6°C over this depth. If valid at cloud base as well as at the height of the UMass W-band scan, the calculated pressure deficit (−4.8 hPa) corresponds to only a 50-m drop in the height of the cloud base in the sounding shown in Fig. 17a. However, funnel 2 clearly extended down farther than 50 m from cloud base; both condensation funnels 1 and 2 exhibited intermittent ground contact (Figs. 1a,b and 4).

By assuming a Rankine vortex structure based on the GBVTD-analyzed RMW, one can obtain the pressure

Downloaded from http://journals.ametsoc.org/mwr/article-pdf/4300712/mwr-d-12-00331_1.pdf by guest on 10 June 2020

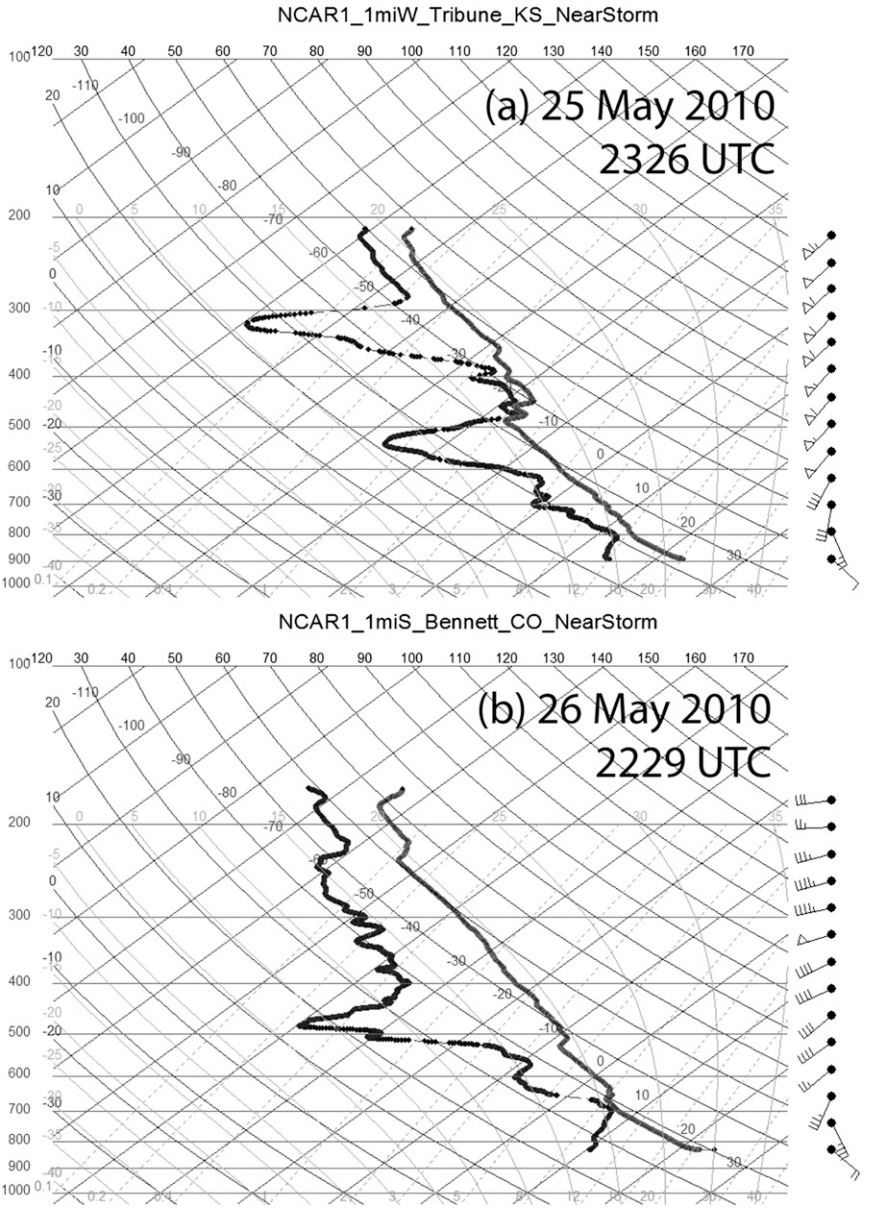

FIG. 17. Mobile rawinsonde observations collected south of (a) the Tribune supercell and (b) the Prospect Valley storm. Temperatures (°C) are plotted along an upper-left-to-lower-right diagonal, while pressure (hPa) is shown on the vertical axis. Wind barbs are plotted in $m\,s^{-1}$ (half barbs $2.5\,m\,s^{-1}$; full barbs $5\,m\,s^{-1}$, and flags $25\,m\,s^{-1}$). The soundings shown are those collected closest to the inflow sector around the time of (a) the tornado or (b) SCVs.

deficit and corresponding V_{T0} needed to overcome the 7.3°C dewpoint depression at 100 m AGL (the height of the UMass W-band scan; Fig. 17a) and thereby form the 30-m-wide condensation funnel pictured in Fig. 4: -21.0 hPa and $46\,m\,s^{-1}$, respectively. As previously discussed, we would not have been able to resolve these inner-core winds in so narrow a funnel using even the high-resolution UMass W-band radar, much less retrieve them using GBVTD.

Possible sources of error in this estimate of V_{T0} are enumerated by Davies-Jones (1986). They include the assumption that ingested air was well represented by the sounding in Fig. 17a. Mobile mesonets operating close to the hook echo before, during, and after the Tribune tornado (not shown) consistently reported that the surface relative humidity was 80%–90%, corresponding to dewpoint depressions of 2°–4°C. Rather than spinning faster at small radii, the tornado could have ingested

Downloaded from http://journals.ametsoc.org/mwr/article-pdf/4300712/mwr-d-12-00331_1.pdf by guest on 10 June 2020

more humid near-surface air, moistening the vortex column and allowing the condensation funnel to form with a more modest pressure deficit than the calculation above suggests.

In summary, trends in V_{T0} outside the condensation funnels indicate increased low-level rotation at all radii when funnels appeared. However, the appearance of condensation funnels could also be explained by the ingestion and lofting of more humid surface air as observed by mobile mesonets. Both possibilities are supported by available evidence. The narrow width and brevity of the cloud-to-ground funnels lead us to believe that the Tribune tornado was barely able to achieve the pressure and temperature drop needed for the funnels to form.

4) ANGULAR MOMENTUM

A number of studies have explored the role of angular momentum transport, particularly that associated with rain curtains, in tornadogenesis (Markowski et al. 2003; Rasmussen and Straka 2007). Rain curtains wrapping around the Tribune tornado were sometimes associated with higher V_T (Figs. 12a–e). While we have only horizontal wind analyses for this case and therefore cannot evaluate vertical transport of angular momentum, it is instructive to examine the relationship of the azimuthally averaged horizontal components of angular momentum per unit mass ($M = V_{T0}r$) and equivalent reflectivity (Fig. 16). In the Tribune tornado, wrapping (quasi-axisymmetric) rain curtains (e.g., dotted circles in Figs. 2b and 2e, respectively) increased the azimuthally averaged reflectivity outside the WEH (e.g., corresponding dotted boxes in Fig. 16) when condensation funnels appeared, and were generally associated with increased M outside the tornado core. However, a rain curtain containing diminished V_T winds (Fig. 12f) passed through the plane of the UMass W-band scan south of funnel 2 at 2322 UTC (Fig. 2f), decreased M at all radii (Fig. 16), and heralded the demise of the Tribune tornado. Therefore, the relationship between rain curtains and angular momentum trends in the Tribune tornado was inconsistent.

5) RMW TRENDS

The RMW (Fig. 18a) was taken as the radius of peak $V_{T0.}$ Prior to tornadogenesis (2314 UTC), we have low confidence in the RMW because the tip of the hook initially contained little precipitation (Fig. 2a), making the returned signal weak and the corresponding Doppler velocities noisy. The RMW fluctuated around 300 m as funnel 1 rapidly filled in with precipitation and matured, and then dissipated at 2317 UTC. Just prior to the appearance of funnel 2 at 2320 UTC, the RMW decreased to about 200 m, then increased again to more than 300 m as funnel 2 dissipated. The trend of decay via increasing RMW and decreasing V_{T0} is consistent with analyses of the Bassett tornado by Bluestein et al. (2003b) and the 31 May 1998 Spencer, South Dakota, tornado by Kosiba and Wurman (2010), but contrasts with results from Tanamachi et al. (2007) and Chan et al. (2012), who found that RMW decreased in the decaying Stockton and Hong Kong International Airport tornadoes, respectively (Table 1). Funnel 2 tilted with height as it dissipated (Fig. 1b), elongating the vortex signature in the UMass W-band data and possibly causing a spurious increase in analyzed RMW. The Basset tornado also tilted with height as it dissipated (Bluestein et al. 2003b; their Fig. 2b). The consistency between changes in analyzed wind speeds and the visual appearance of the condensation funnel lends confidence to the analyzed trends in V_{T0}. The Tribune tornado appears to have been more like the Bassett tornado than the Stockton tornado in most regards. Because the Tribune and Bassett tornadoes are similar in terms of their strength and tilt during the rope-out phase, it is not surprising that the two also exhibit similar increases in RMW as azimuthal winds decreased.

b. 26 May 2010: SCV 5 near Prospect Valley, Colorado

We analyzed the UMass W-band data collected in SCV 5 in exactly the same manner as we did previous UMass W-band tornado datasets. We were able to retrieve V_T and V_R components of flow in the SCV using GBVTD once the developing SCV 5 (initially scatterer-free) was completely encircled by scatterers at genesis (2234 UTC), leaving a WEH in the middle (Fig. 9a). It is possible that a vortex was present prior to this time but not detected by UMass W band for lack of scatterers.

Overall, SCV 5's analyzed V_{T0} structure was similar to that of the Tribune tornado (Fig. 19). At peak intensity (2238 UTC), the axisymmetric wind profile was reminiscent of a Burgers–Rott vortex with peak $V_{T0} \sim 13\,\mathrm{m\,s^{-1}}$ Fig. 20d) at a radius of 80 m. The V_{T1} and V_{T2} asymmetries were consistently embedded in curtains of precipitation that wrapped around SCV 5 (with respect to the UMass W band). Over its 8-min life cycle, SCV 5 intensified and then decayed in a manner similar to previously analyzed tornadoes. However, weaker axisymmetric azimuthal velocities were analyzed in TLV 5 (Fig. 21) than in the Tribune, Bassett, or Stockton tornadoes.

1) AXISYMMETRIC WINDS

Radial inflow (approximately $-2\,\mathrm{m\,s^{-1}}$) was analyzed outside the vortex core as SCV 5 intensified

Downloaded from http://journals.ametsoc.org/mwr/article-pdf/4300712/mwr-d-12-00331_1.pdf by guest on 10 June 2020

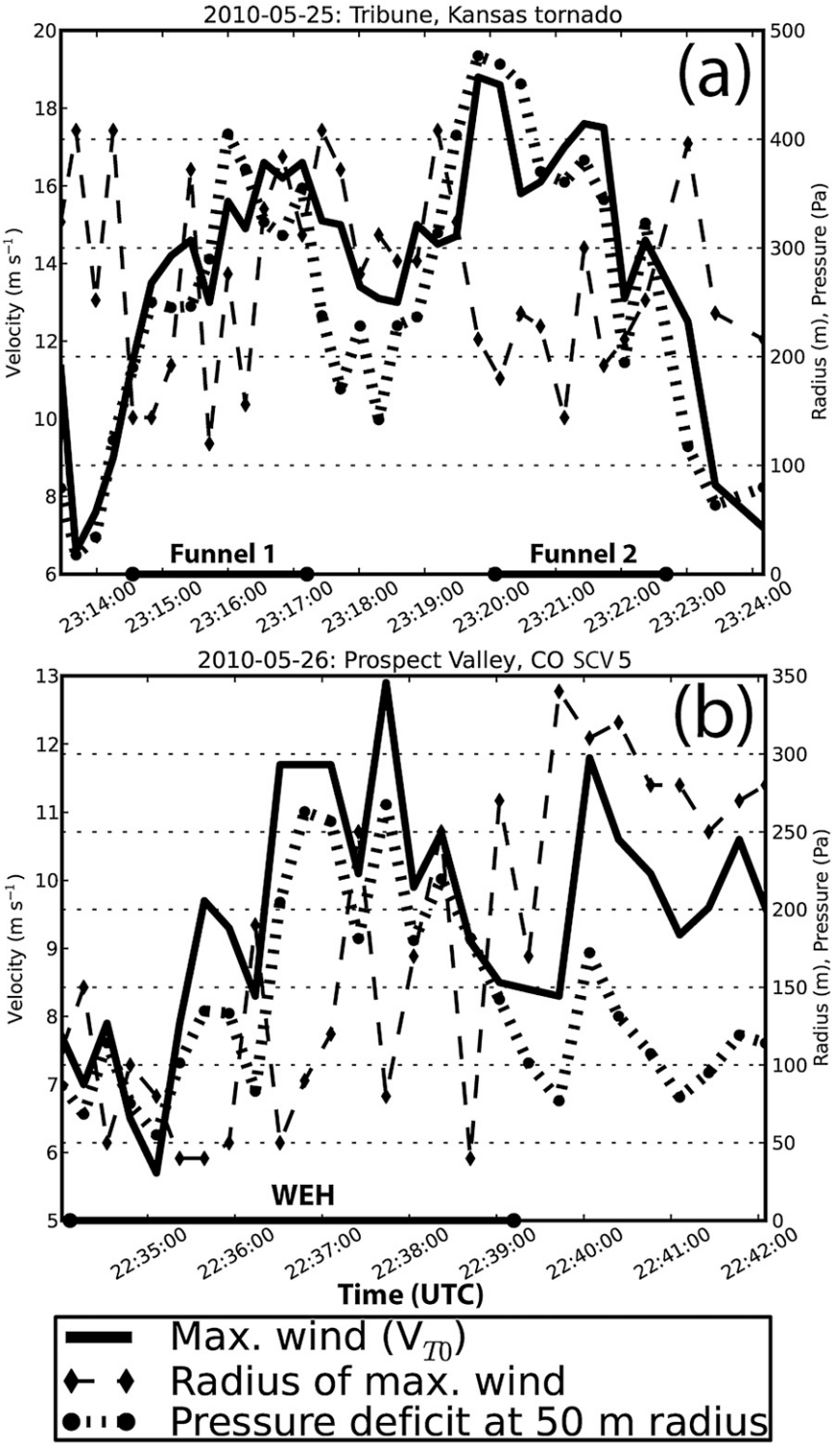

FIG. 18. (a) Maximum V_{T0} (solid line, m s^{-1}), radius of maximum V_{T0} (dashed line connecting diamonds, m), and integrated cyclostrophic pressure deficit at 50-m radius (dotted line connecting circles, Pa) analyzed in the Tribune tornado. The appearances of condensation funnels are annotated on the horizontal axis. (b) As in (a), but for Prospect Valley SCV 5. The WEH is annotated on the horizontal axis.

Downloaded from http://journals.ametsoc.org/mwr/article-pdf/4300712/mwr-d-12-00331_1.pdf by guest on 10 June 2020

TABLE 1. Summary of GBVTD-analyzed RMW changes during the intensification and decay phases of tornadoes observed by Doppler radars. For the Tribune tornado, the two arrows correspond to the two condensation funnels.

	Tornado					
	Stockton, KS	Bassett, NE	Tribune, KS	Prospect Valley, CO, SCV 5	Spencer, SD	Hong Kong International Airport
Reference	Tanamachi et al. (2007)	Bluestein et al. (2003b)	This manuscript	This manuscript	Kosiba and Wurman (2010)	Chan et al. (2012)
Rating	F1	F0	EF0	<EF0	F5	F0
Radar	UMass W band	UMass W band	UMass W band	UMass W band	DOW	Terminal Doppler Weather Radar
Analysis altitude (AGL)	100–150 m	250 m	100 m	150 m	40 m	160 m
RMW trend during genesis	↔	↓	↓↓	↓	Not covered	↓
RMW trend during decay	↓	↑	↑↑	↔	↑	↓

(2234–2238 UTC) and again as it dissipated (2240–2242 UTC), with a brief period of radial outflow ($\sim$4 m s^{-1}) in between (2238–2240 UTC). Although outflow was analyzed at most times at the innermost radii (<100 m), we again caution that, even though SCV 5's WEH was smaller, V_{R0} was based on a relatively small number of data points and was likely contaminated by centrifuging of hydrometeors (Wakimoto et al. 2012; Nolan 2013).

Lacking a condensation funnel to use as an indicator of vortex intensification, we instead took the presence of a WEH as an indicator of intense winds in the SCV core (Dowell et al. 2005). The WEH, continuously present from 2234 to 2239 UTC, was about half as wide ($\sim$100-m diameter) as that in the Tribune tornado (Fig. 16). The WEH widened in concert with the highest analyzed V_{T0} in the SCV (Fig. 22), an observation consistent with increased centrifuging of hydrometeors at low levels (Tanamachi et al. 2012). After briefly filling in with precipitation at 2239 UTC, the WEH opened up again from 2240 to 2242 UTC (Fig. 22) as SCV 5 fell behind the larger-scale hook structure and dissipated (Figs. 2 and 11).

2) RMW TRENDS

Vorticity in the core of SCV 5 was $\sim$0.3 s^{-1} (comparable to or even exceeding that found in some tornadoes) whenever the WEH was present (Fig. 23). Circulation generally increased (decreased) at all radii when SCV 5 intensified (weakened; Fig. 23). The RMW shrank to less than 100 m as SCV 5 intensified (2234–2238 UTC), then increased beyond 200 m after the WEH closed at 2240 UTC (Fig. 18b). This inverse relationship of V_{T0} and RMW is consistent with that found in previously analyzed tornadoes, including the Tribune tornado (Table 1). Somewhat oddly, vorticity in SCV 5 appeared to increase as it dissipated at 2242 UTC. This increase in vorticity may have been associated with another SCV (7; Figs. 7k,l) that formed less than a minute after and within 1 km of where SCV 5 dissipated (Fig. 8).

3) ABSENCE OF A CONDENSATION FUNNEL

It appears that the air underneath the hook echo was simply too dry for the formation of a condensation funnel. A sounding launched in the inflow sector of the Prospect Valley storm (Fig. 17b) contains dewpoint depressions ranging from 12.3°C near the surface (830 hPa) to 0.3°C at the top of the well-mixed layer (690 hPa, or 1.6 km AGL). As in the Tribune storm, the air near the surface was moister than indicated by the sounding shown in Fig. 17b. Measurements of relative humidity from mobile mesonets in the inflow sector were 55%–75%, corresponding to surface dewpoint depressions of 5°–9°C. However, these dewpoint depressions were still considerably larger than those observed beneath the Tribune storm. If we assume, as we did for the Tribune tornado, that SCV 5 was in cyclostrophic balance, the pressure and temperature deficits resulting from the analyzed V_{T0} winds (which peaked at 13 m s^{-1}) would have been $-$2.7 hPa (Fig. 18b) and $-$1.0°C, respectively, lowering the cloud base overhead by only about 32 m (Fig. 1c). To overcome a 9°C dewpoint depression, allowing a funnel to reach the ground, a Rankine vortex with the same RMW would have required maximum axisymmetric azimuthal winds of 51 m s^{-1}, a scenario that we consider unlikely since no surface damage or condensation funnel were observed and because Doppler velocity observations in the vortex did not reach this value (Figs. 1c,d). We suspect that the inner core of the vortex contained more intense winds than those analyzed outside the core using GBVTD, and that these winds were responsible for the WEH.

Downloaded from http://journals.ametsoc.org/mwr/article-pdf/4300712/mwr-d-12-00331_1.pdf by guest on 10 June 2020

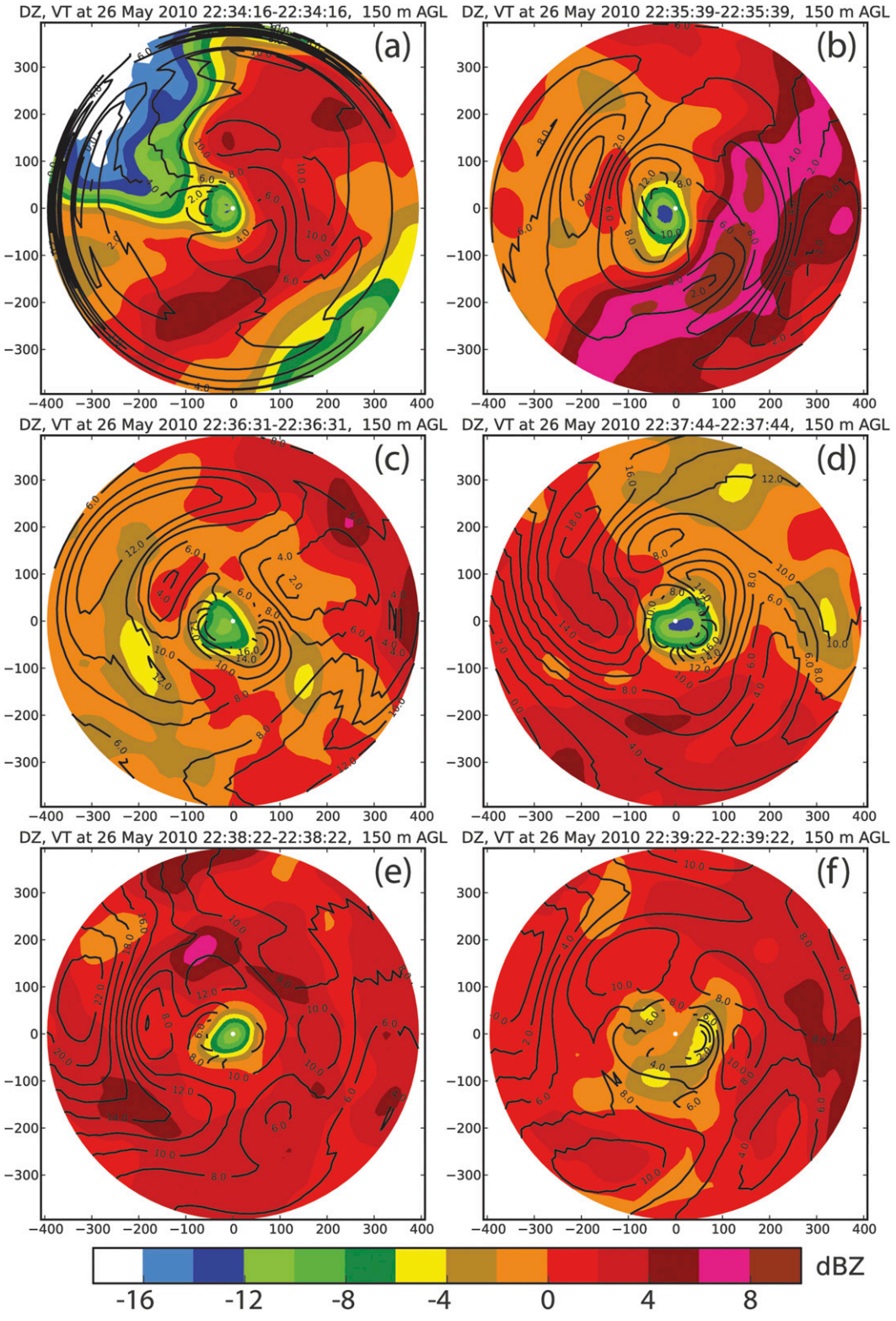

FIG. 19. As in Fig. 12, but for SCV 5 in the 26 May 2010 Prospect Valley storm at (a) 2234, (b) 2236, (c) 2237, (d) 2338, (e) 2238, and (f) 2339 UTC.

Downloaded from http://journals.ametsoc.org/mwr/article-pdf/4300712/mwr-d-12-00331_1.pdf by guest on 10 June 2020

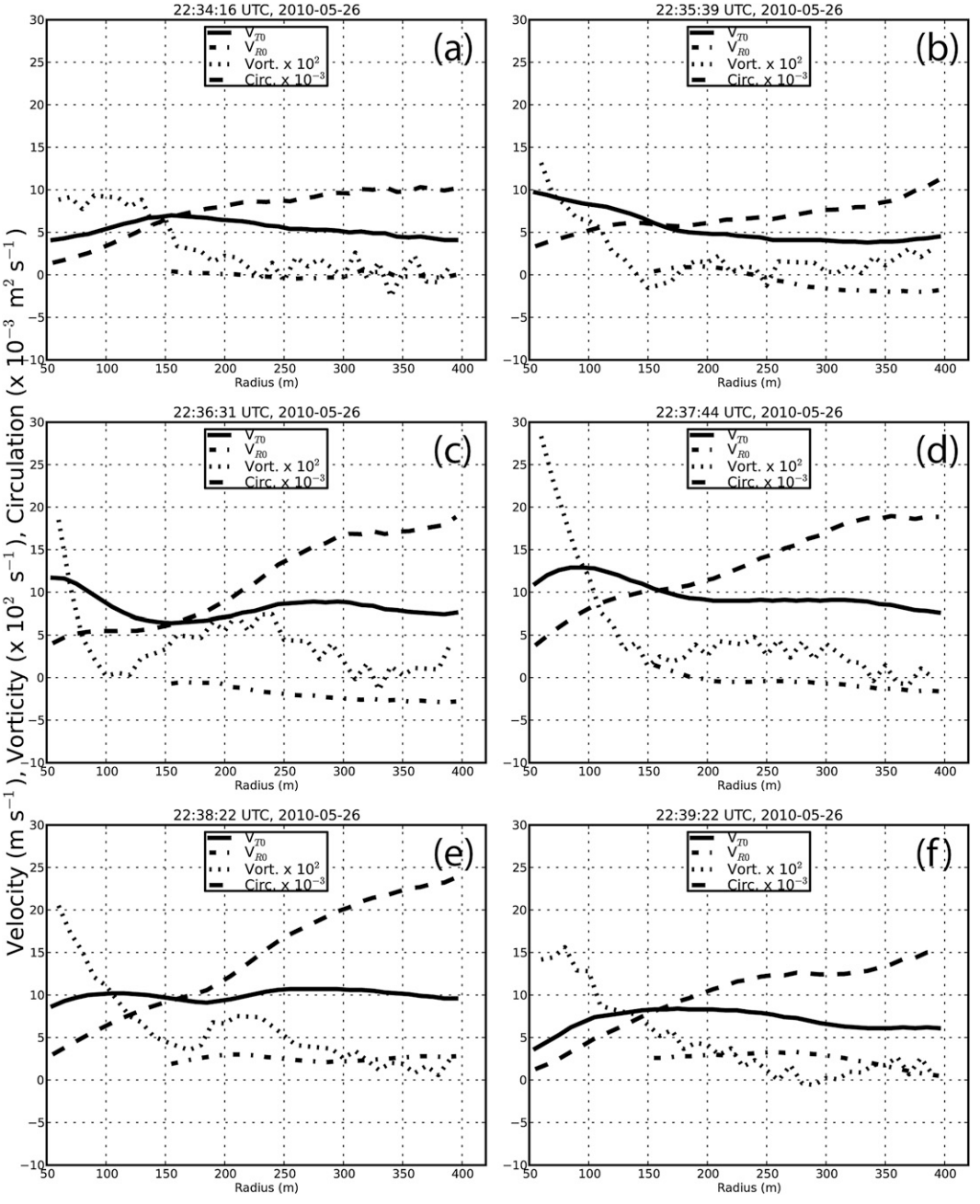

FIG. 20. As in Fig. 13, but for the analyses shown in Fig. 19.

However, the resulting dynamic pressure drop in the inner core was not sufficient to form a condensation funnel.

5. Conclusions

High-resolution (~10 m) GBVTD analyses were conducted on two W-band radar datasets collected in the hook echoes of tornadic supercells during VORTEX2. The two datasets, collected one day apart and less than 200 m above the surface, show the full life cycle of an EF-0 tornado in western Kansas and a SCV, which did not have an associated condensation funnel, in northeast Colorado. Although both vortices satisfied a radar-based criterion for a tornado, the latter lacked visual features that would have identified it as a tornado to human observers.

The Tribune tornado appeared as a series of two condensation funnels, separated in time by about 3 min.

Downloaded from http://journals.ametsoc.org/mwr/article-pdf/4300712/mwr-d-12-00331_1.pdf by guest on 10 June 2020

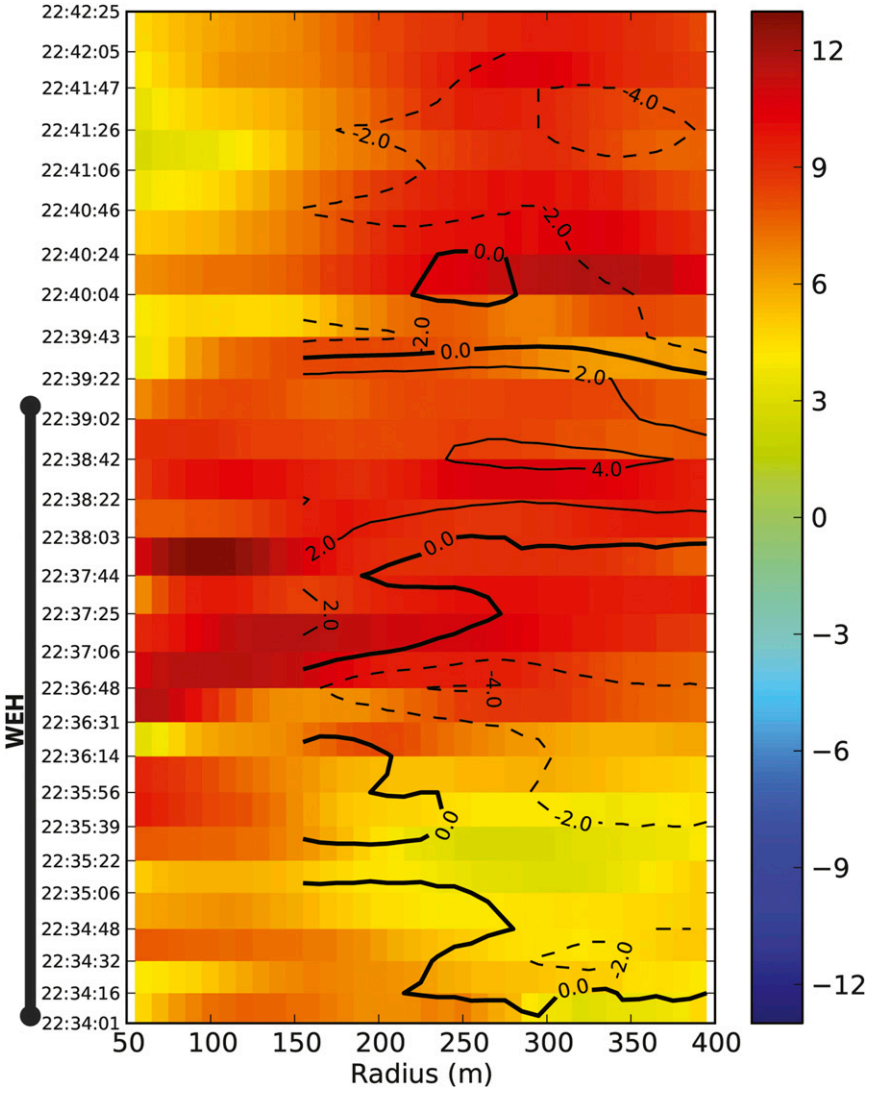

FIG. 21. As in Fig. 14, but for Prospect Valley SCV 5. The presence of the WEH is denoted on the vertical axis.

In the UMass W-band data, the WEH and VS of the Tribune tornado persisted through the time gap between the two condensation funnels (Fig. 2, Fig. 3). GBVTD-analyzed azimuthal velocities, circulation, and vorticity increased (decreased) when the funnel clouds appeared (disappeared). The maximum V_{T0} and its radius were inversely related, particularly during the appearance of funnel 2 (Fig. 18a), as has been found in previously analyzed tornadoes.

It was found that the Tribune tornado and Prospect Valley SCV 5 both had similar radar presentations (in terms of a persistent VS, WEH, and convergent spiral bands of reflectivity), life spans (as measured by the appearance of WEHs; ~8 min), intensification and weakening phases (as seen in the evolution of the RMW, circulation/angular momentum, and vorticity), and axisymmetric vortex structure at peak intensity. A VS and WEH are clearly visible in the UMass W-band data collected in SCV 5 on 26 May 2010, and they bear a strong resemblance to those seen in the Tribune tornado the previous day. Vorticity in SCV 5 (~0.3 s^{-1}) was comparable to that analyzed in the Tribune tornado and other previously documented tornadoes. The principal differences between these two vortices lie in the speed of the azimuthal winds (which were smaller for the SCV), the RMW (which was wider in the Tribune tornado), and the absence of a condensation funnel in SCV 5, which we attribute to inadequate moisture below cloud base (Fig. 17b).

It is well known that a tornado with no visible condensation funnel can still inflict surface damage (although

Downloaded from http://journals.ametsoc.org/mwr/article-pdf/4300712/mwr-d-12-00331_1.pdf by guest on 10 June 2020

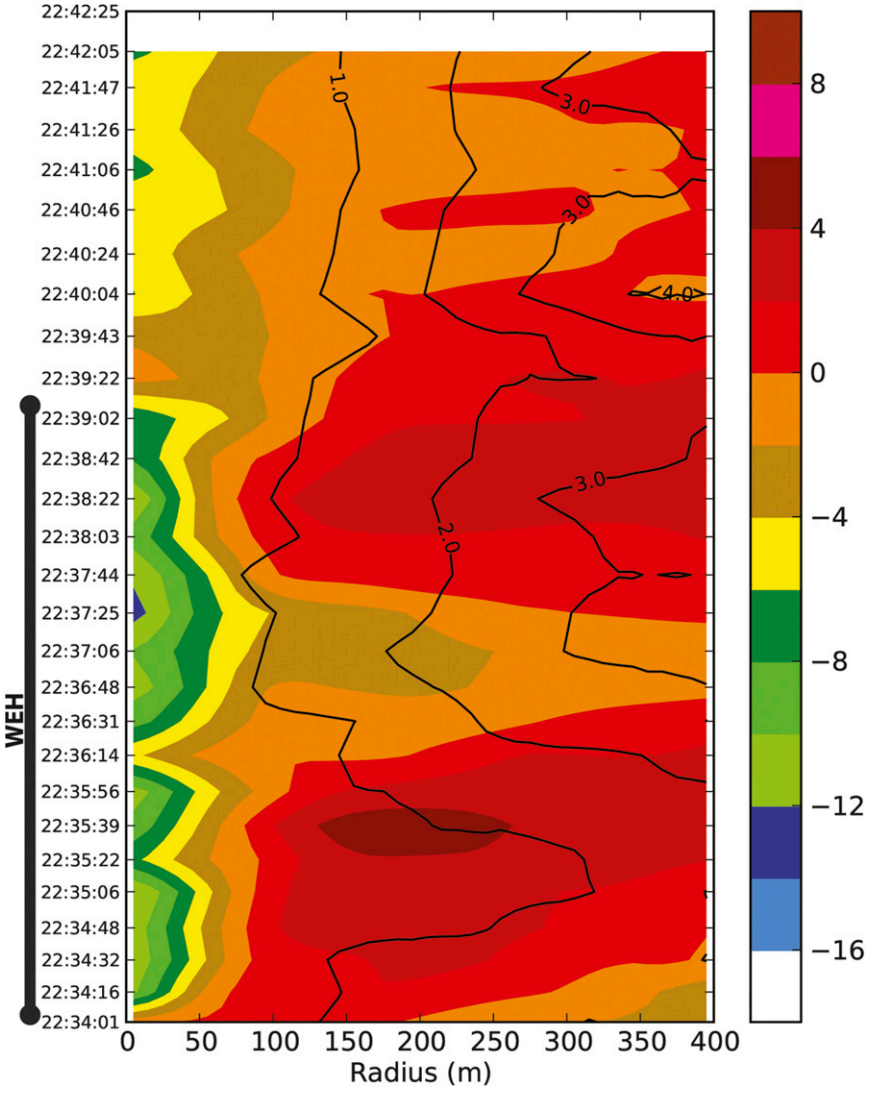

FIG. 22. As in Fig. 16, but for Prospect Valley SCV 5.

none was documented in this case). The motion of SCV 5 (Fig. 11) was likely influenced by a submesocyclone scale circulation that was documented by other VORTEX2 radars (Fig. 5b), and it occurred in conjunction with other features frequently accompanying mesocyclonic tornadoes (e.g., a clear slot). Therefore, it is unlikely that SCV 5 was a nonmesocyclonic vortex or a ''gustnado.''

While the peak analyzed V_{T0} in the Prospect Valley SCV 5 was only $13\,m\,s^{-1}$, peak analyzed V_{T0} in the Tribune, Bassett, and Stockton tornadoes approached or even dipped below this value at some point during their life cycles. In addition, similar velocities were measured by UMass W band at inner radii in both the Tribune tornado and SCV 5. Although SCV 5, which exhibited a persistent low-level VS and WEH in an expected location for a tornado, met the Alexander and Wurman (2008) criterion, none of the more than 100 VORTEX2 personnel, most of whom had at least some tornado field research experience, identified it as a tornado or even a funnel cloud, only a ''suspicious lowering'' of the cloud base (Fig. 1c).

We suspect that many such SCVs occur beneath high plains supercells but go undetected. High-resolution radars such as the UMass W band, Texas Tech University Ka-band mobile radars (Hirth et al. 2012), and X-band mobile radars (e.g., Wurman et al. 1997; Kramar et al. 2005; Burgess et al. 2010) at similarly close range (i.e., a few kilometers) are best suited for detecting and documenting such vortices.

This study adds to a growing list of GBVTD-based studies of high-resolution mobile Doppler radar data collected in tornadoes. While the tornado and SCV

Downloaded from http://journals.ametsoc.org/mwr/article-pdf/4300712/mwr-d-12-00331_1.pdf by guest on 10 June 2020

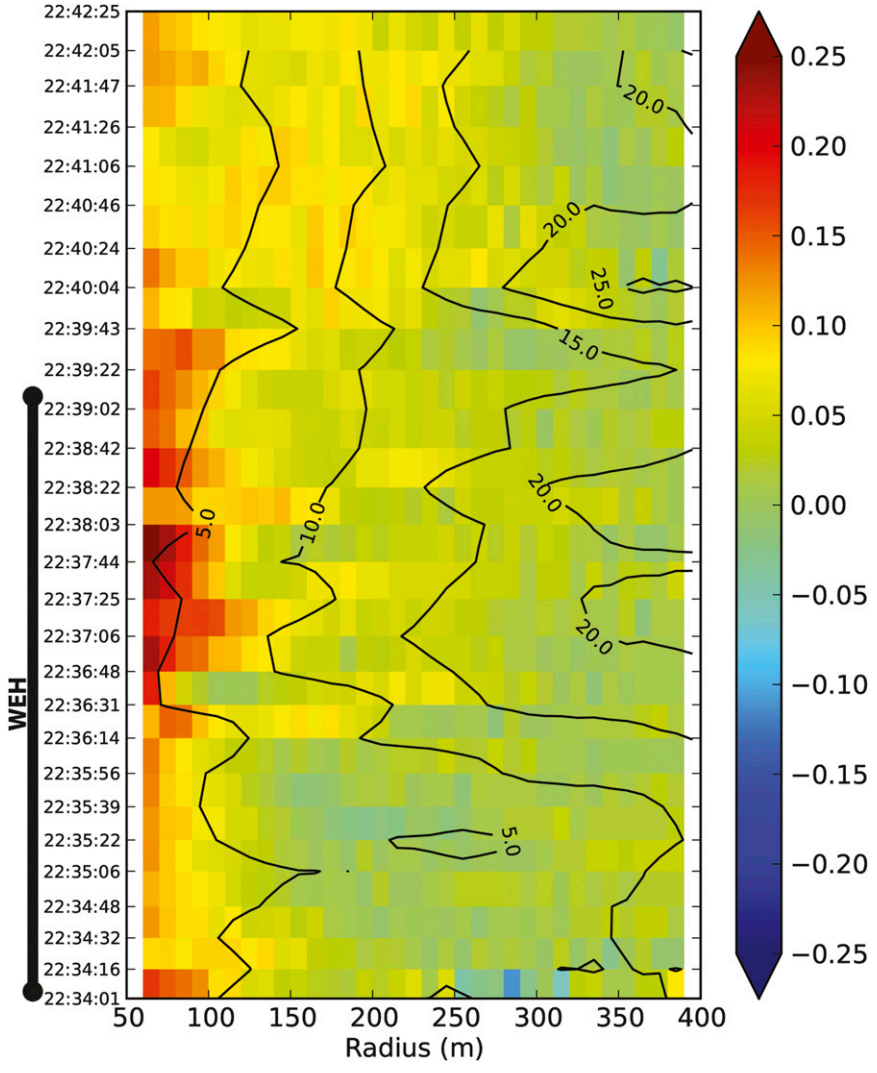

FIG. 23. As in Fig. 15, but for Prospect Valley SCV 5.

analyzed here could be considered minimal tornadoes, the results of the GBVTD analyses suggest that they share many features in common with stronger tornadoes. It is believed this is the first time the full life cycle of a SCV has been formally documented in the literature using high-resolution Doppler radar data collected beneath a supercell that previously produced tornadoes. We offer our findings in an effort to develop a better understanding of the variability in vortex structure across the tornado spectrum.

Acknowledgments. This study was primarily supported by National Science Foundation (NSF) Grant AGS-0802888. The UMass W-band and MWR-05XP radar data collection during VORTEX2 was supported by NSF Grants ATM-0934307, AGS-0641201, and AGS-0937768, and occurred while the first author was a graduate student at the OU School of Meteorology. Observation Processing and Wind Synthesis (OPAWS; http://code.google.com/p/opaws/) software created by Drs. David Dowell and Louis Wicker was used for the objective analyses. Drs. Phillip Stauffer and Michael Bell updated the GBVTD code. Chad Baldi, Dr. Mike French, and Jana Houser collected and processed the MWR-05XP data with support from Robert Bluth. A manuscript by Mingjun Wang, Dr. Kun Zhao, and collaborators on a gradient velocity track display (GrVTD) algorithm provided initial motivation for this study. Sounding and mobile mesonet data from VORTEX2 were provided by the National Center for Atmospheric Research Earth Observing Laboratory (NCAR/EOL) under sponsorship of the NSF. We are grateful for illuminating conversations with Don Burgess and Vincent "Bim" Wood. GBVTD results were plotted using Matplotlib for

Downloaded from http://journals.ametsoc.org/mwr/article-pdf/4300712/mwr-d-12-00331_1.pdf by guest on 10 June 2020

Python (http://matplotlib.org/). Insightful feedback from Dr. David Lewellen and two other anonymous reviewers substantially improved this manuscript.

REFERENCES

Agee, E. M., J. T. Snow, and P. R. Clare, 1976: Multiple vortex features in the tornado cyclone and the occurrence of tornado families. *Mon. Wea. Rev.,* **104,** 552–563.

Alexander, C. R., 2010: A mobile radar based climatology of supercell tornado structures and dynamics. Ph.D. dissertation, School of Meteorology, University of Oklahoma, 251 pp.

——, and J. Wurman, 2008: Updated mobile radar climatology of supercell tornado structures and dynamics. *Extended Abstracts, 24th Conf. on Severe Local Storms,* Savannah, GA, Amer. Meteor. Soc., 19.4. [Available online at https://ams.confex.com/ams/24SLS/techprogram/paper_141821.htm.]

Atkins, N. T., A. McGee, R. Ducharme, R. M. Wakimoto, and J. Wurman, 2012: The LaGrange tornado during VORTEX 2. Part II: Photogrammetric analysis of the tornado combined with dual-Doppler radar data. *Mon. Wea. Rev.,* **140,** 2939–2958.

Barnes, S. L., 1964: A technique for maximizing details in numerical weather map analysis. *J. Appl. Meteor.,* **3,** 396–409.

Bluestein, H. B., and A. L. Pazmany, 2000: Observations of tornadoes and other convective phenomena with a mobile, 3-mm wavelength, Doppler radar: The spring 1999 field experiment. *Bull. Amer. Meteor. Soc.,* **81,** 2939–2952.

——, C. C. Weiss, and A. L. Pazmany, 2001: Observations in supercells with a mobile, 3-mm wavelength Doppler radar. Preprints, *30th Int. Conf. on Radar Meteorology,* Munich, Germany, Amer. Meteor. Soc., 292–294.

——, ——, and ——, 2003a: Mobile Doppler radar observations of a tornado in a supercell near Bassett, Nebraska, on 5 June 1999. Part I: Tornadogenesis. *Mon. Wea. Rev.,* **131,** 2954–2967.

——, W.-C. Lee, M. Bell, C. C. Weiss, and A. L. Pazmany, 2003b: Mobile Doppler radar observations of a tornado in a supercell near Bassett, Nebraska, on 5 June 1999. Part II: Tornado-vortex structure. *Mon. Wea. Rev.,* **131,** 2968–2984.

——, C. C. Weiss, M. M. French, E. M. Holthaus, R. L. Tanamachi, S. Frasier, and A. L. Pazmany, 2007: The structure of tornadoes near Attica, Kansas, on 12 May 2004: High-resolution, mobile, Doppler radar observations. *Mon. Wea. Rev.,* **135,** 475–506.

——, M. M. French, I. PopStefanija, R. T. Bluth, and J. B. Knorr, 2010: A mobile, phased-array Doppler radar for the study of severe convective storms. *Bull. Amer. Meteor. Soc.,* **91,** 579–600.

Browning, K. A., and R. J. Donaldson, 1963: Airflow and structure of a tornadic storm. *J. Atmos. Sci.,* **20,** 533–545.

Burgers, J. M., 1948: A mathematical model illustrating the theory of turbulence. *Adv. Appl. Mech.,* **1,** 171–199.

Burgess, D. W., M. A. Magsig, J. Wurman, D. C. Dowell, and Y. Richardson, 2002: Radar observations of the 3 May 1999 Oklahoma City tornado. *Wea. Forecasting,* **17,** 456–471.

——, E. R. Mansell, C. Schwarz, and B. Allen, 2010: Tornado and tornadogenesis events seen by the NOXP X-band, dual-polarization radar during VORTEX2 2010. *Extended Abstracts, 25th Conf. on Severe Local Storms,* Denver, CO, Amer. Meteor. Soc., 5.2. [Available online at https://ams.confex.com/ams/25SLS/webprogram/Paper176164.html.]

Carbone, R. E., M. J. Carpenter, and C. D. Burghart, 1985: Doppler radar sampling limitations in convective storms. *J. Atmos. Oceanic Technol.,* **2,** 357–361.

Chan, P. W., J. Wurman, C. M. Shun, P. Robinson, and K. Kosiba, 2012: Application of a method for the automatic detection and ground-based velocity track display (GBVTD) analysis of a tornado crossing the Hong Kong International Airport. *Atmos. Res.,* **106,** 18–29.

Davies-Jones, R., 1986: Tornado dynamics. *Thunderstorm Morphology and Dynamics,* 2nd ed. E. Kessler, Ed., University of Oklahoma Press, 197–236.

Doviak, R. J., D. Sirmans, D. S. Zrnić, and G. Walker, 1976: Resolution of pulse-Doppler radar range and velocity ambiguities in severe storms. Preprints, *17th Conf. on Radar Meteorology,* Seattle, WA, Amer. Meteor. Soc., 15–22.

Dowell, D. C., C. R. Alexander, J. M. Wurman, and L. J. Wicker, 2005: Centrifuging of hydrometeors and debris in tornadoes: Radar-reflectivity patterns and wind-measurement errors. *Mon. Wea. Rev.,* **133,** 1501–1524.

Fujita, T., 1960: A detailed analysis of the Fargo tornadoes of June 20, 1957. U.S. Weather Bureau Research Paper 42, 67 pp.

——, 1971: Proposed characterization of tornadoes and hurricanes by area and intensity. Satellite and Mesometeorology Research Project, Research Paper 91, University of Chicago, 42 pp.

Glickman, T. S., 2000: *Glossary of Meteorology.* 2nd ed. Amer. Meteor. Soc., 855 pp.

Hirth, B. D., J. L. Schroeder, W. S. Gunter, and J. G. Guynes, 2012: Measuring a utility-scale turbine wake using the TTUKa mobile research radars. *J. Atmos. Oceanic Technol.,* **29,** 765–771.

Koch, S. E., M. desJardins, and P. J. Kocin, 1983: An interactive Barnes objective map analysis scheme for use with satellite and conventional data. *J. Climate Appl. Meteor.,* **22,** 1487–1503.

Kosiba, K., and J. Wurman, 2010: The three-dimensional axisymmetric wind field structure of the Spencer, South Dakota, 1998 tornado. *J. Atmos. Sci.,* **67,** 3074–3083.

——, R. J. Trapp, and J. Wurman, 2008: An analysis of the axisymmetric three-dimensional low level wind field in a tornado using mobile radar observations. *Geophys. Res. Lett.,* **35,** L05805, doi:10.1029/2007GL031851.

——, J. Wurman, Y. Richardson, P. Markowski, P. Robinson, and J. Marquis, 2013: Genesis of the Goshen County, Wyoming, tornado on 5 June 2009 during VORTEX2. *Mon. Wea. Rev.,* **141,** 1157–1181.

Kramar, M. R., H. B. Bluestein, A. L. Pazmany, and J. D. Tuttle, 2005: The ''owl horn'' radar signature in developing southern Plains supercells. *Mon. Wea. Rev.,* **133,** 2608–2634.

Lee, W.-C., and F. D. Marks, 2000: Tropical cyclone kinematic structure retrieved from single-Doppler radar observations. Part II: The GBVTD-simplex center finding algorithm. *Mon. Wea. Rev.,* **128,** 1925–1936.

——, and J. Wurman, 2005: Diagnosed three-dimensional axisymmetric structure of the Mulhall tornado on 3 May 1999. *J. Atmos. Sci.,* **62,** 2373–2393.

——, B. J.-D. Jou, P.-L. Chang, and S.-M. Deng, 1999: Tropical cyclone kinematic structure retrieved from single-Doppler radar observations. Part I: Interpretation of Doppler velocity patterns and the GBVTD technique. *Mon. Wea. Rev.,* **127,** 2419–2439.

Lemon, L. R., and C. A. Doswell, 1979: Severe thunderstorm evolution and mesocyclone structure as related to tornadogenesis. *Mon. Wea. Rev.,* **107,** 1184–1197.

Majcen, M., P. Markowski, Y. Richardson, D. Dowell, and J. Wurman, 2008: Multipass objective analyses of Doppler radar data. *J. Atmos. Oceanic Technol.,* **25,** 1845–1858.

Downloaded from http://journals.ametsoc.org/mwr/article-pdf/4300712/mwr-d-12-00331_1.pdf by guest on 10 June 2020

Markowski, P. M., J. M. Straka, and E. N. Rasmussen, 2003: Tornadogenesis resulting from the transport of circulation by a downdraft: Idealized numerical simulations. *J. Atmos. Sci.,* **60,** 795–823.

Marquis, J., Y. Richardson, P. Markowski, D. Dowell, and J. Wurman, 2012: Tornado maintenance investigated with high-resolution dual-Doppler and EnKF analysis. *Mon. Wea. Rev.,* **140,** 3–27.

McDonald, J. R., and K. C. Mehta, 2006: A recommendation for an Enhanced Fujita Scale (EF-Scale). Texas Tech University, Lubbock, Texas, 111 pp. [Available online at http://www.depts.ttu.edu/nwi/Pubs/FScale/Fujita.php.]

Metzger, R. S., C. C. Weiss, and A. E. Reinhart, 2011: An examination of the structure of three tornadoes using high-frequency Ka-band mobile Doppler radar. *Extended Abstracts, 35th Conf. on Radar Meteorology,* Pittsburgh, PA, Amer. Meteor. Soc., 7B.4. [Available online at https://ams.confex.com/ams/35Radar/webprogram/Paper191774.html.]

Monteverdi, J. P., M. M. Umscheid, and E. M. Bookbinder, 2010: Two tornadic thunderstorms in ostensibly weak deep layer shear environments in southeastern Colorado: cyclic supercells of May 25 (Kiowa County) and May 31 (Baca County) 2010. *Extended Abstracts, 25th Conf. on Severe Local Storms,* Denver, CO, Amer. Meteor. Soc., P10.14. [Available online at https://ams.confex.com/ams/25SLS/techprogram/paper_175862.htm.]

National Climatic Data Center, cited 2011: Storm events database. [Available online at http://www.ncdc.noaa.gov/stormevents/.]

Nelder, J. A., and R. Mead, 1965: A simplex method for function minimization. *Comput. J.,* **7,** 308–313.

Nolan, D. S., 2013: On the use of Doppler radar–derived wind fields to diagnose the secondary circulations of tornadoes. *J. Atmos. Sci.,* **70,** 1160–1171.

Pauley, P. M., and X. Wu, 1990: The theoretical, discrete, and actual response of the Barnes objective analysis scheme for one- and two-dimensional fields. *Mon. Wea. Rev.,* **118,** 1145–1164.

Rasmussen, E. N., and J. M. Straka, 2007: Evolution of low-level angular momentum in the 2 June 1995 Dimmitt, Texas, tornado cyclone. *J. Atmos. Sci.,* **64,** 1365–1378.

Rott, N., 1958: On the viscous core of a line vortex. *Z. Angew. Math. Phys.,* **9,** 543–553.

Schenkman, A. D., M. Xue, and A. Shapiro, 2012: Tornadogenesis in a simulated mesovortex within a mesoscale convective system. *J. Atmos. Sci.,* **69,** 3372–3390.

Sirmans, D., D. S. Zrnić, and B. Bumgarner, 1976: Extension of maximum unambiguous Doppler velocity by use of two sampling rates. Preprints, *17th Conf. on Radar Meteorology,* Seattle, WA, Amer. Meteor. Soc., 23–28.

Snyder, J. C., R. L. Tanamachi, H. B. Bluestein, W.-C. Lee, M. Bell, and A. Pazmany, 2006: Reconstruction of wind profiles in dust devils: Analyses of W-band mobile radar data using the ground-based velocity track display (GBVTD) technique. *Extended Abstracts, 23rd Conf. on Severe Local Storms,* St. Louis, MO, Amer. Meteor. Soc., P9.6. [Available online at https://ams.confex.com/ams/23SLS/techprogram/paper_115434.htm.]

Straka, J. M., E. N. Rasmussen, R. P. Davies-Jones, and P. M. Markowski, 2007: An observational and idealized numerical examination of low-level counter-rotating vortices in the rear flank of supercells. *Electron. J. Severe Storms Meteor.,* **2,** 1–22.

Sullivan, R. D., 1959: A two-cell vortex solution of the Navier–Stokes equations. *J. Aerosp. Sci.,* **26,** 767–768.

Tanamachi, R. L., H. B. Bluestein, W.-C. Lee, M. Bell, and A. Pazmany, 2007: Ground-based velocity track display (GBVTD) analysis of W-band Doppler radar data in a tornado near Stockton, Kansas, on 15 May 1999. *Mon. Wea. Rev.,* **135,** 783–800.

——, ——, J. B. Houser, K. M. Hardwick, and S. J. Frasier, 2012: Mobile, X-band, polarimetric Doppler radar observations of the 4 May 2007 Greensburg, Kansas tornadic supercell. *Mon. Wea. Rev.,* **140,** 2103–2125.

Trapp, R. J., and C. A. Doswell, 2000: Radar data objective analysis. *J. Atmos. Oceanic Technol.,* **17,** 105–120.

Tsai, P., S. Frasier, R. L. Tanamachi, and H. B. Bluestein, 2008: The UMass mobile W-Band Doppler radar: System overview and sample observations. Preprints, *24th Conf. on Severe Local Storms,* Savannah, GA, Amer. Meteor. Soc., P13.5. [Available online at https://ams.confex.com/ams/24SLS/techprogram/paper_142152.htm.]

Wakimoto, R. M., N. T. Atkins, and J. Wurman, 2011: The LaGrange tornado during VORTEX2. Part I: Photogrammetric analysis of the tornado combined with single-Doppler radar data. *Mon. Wea. Rev.,* **139,** 2233–2258.

——, P. Stauffer, W.-C. Lee, N. T. Atkins, and J. Wurman, 2012: Finescale structure of the LaGrange, Wyoming, tornado during VORTEX2: GBVTD and photogrammetric analyses. *Mon. Wea. Rev.,* **140,** 3397–3418.

Weiss, C. C., J. L. Schroeder, J. G. Guynes, P. S. Skinner, and J. Beck, 2009: The TTUKa mobile Doppler radar: Coordinated radar and in situ measurements of supercell thunderstorms during Project VORTEX2. *Extended Abstracts, 34th Conf. on Radar Meteorology,* Williamsburg, VA, Amer. Meteor. Soc., 11B.2. [Available online at https://ams.confex.com/ams/34Radar/webprogram/Paper155425.html.]

Wurman, J., and C. R. Alexander, 2005: The 30 May 1998 Spencer, South Dakota, storm. Part II: Comparison of observed damage and radar-derived winds in the tornadoes. *Mon. Wea. Rev.,* **133,** 97–119.

——, and K. A. Kosiba, 2008: DOW observations of multiple vortex structure in several tornadoes. *Extended Abstracts, 24th Conf. on Severe Local Storms,* Savannah, GA, Amer. Meteor. Soc., P3.20. [Available online at https://ams.confex.com/ams/24SLS/techprogram/paper_142194.htm.]

——, J. Straka, E. Rasmussen, M. Randall, and A. Zahrai, 1997: Design and deployment of a portable, pencil-beam, pulsed, 3-cm Doppler radar. *J. Atmos. Oceanic Technol.,* **14,** 1502–1512.

——, D. Dowell, Y. Richardson, P. Markowski, E. Rasmussen, D. Burgess, L. Wicker, and H. B. Bluestein, 2012: The Second Verification of the Origins of Rotation in Tornadoes Experiment: VORTEX2. *Bull. Amer. Meteor. Soc.,* **93,** 1147–1170.

——, K. Kosiba, and P. Robinson, 2013: In situ, Doppler radar, and video observations of the interior structure of a tornado and the wind–damage relationship. *Bull. Amer. Meteor. Soc.,* **94,** 835–846.

Downloaded from http://journals.ametsoc.org/mwr/article-pdf/4300712/mwr-d-12-00331_1.pdf by guest on 10 June 2020